

ste Lib Copy

4

ESD RECORD COPY

RETURN TO
SCIENTIFIC & TECHNICAL INFORMATION DIVISION
(ESTI), BUILDING 3000

Solid State Research

NOV
1969

Prepared under Electronic Systems Division Contract AF 19(628)-5167 by

Lincoln Laboratory

MASSACHUSETTS INSTITUTE OF TECHNOLOGY

Lexington, Massachusetts



AD0701022

This document has been approved for public release and sale;
its distribution is unlimited.

4

Solid State Research

1969

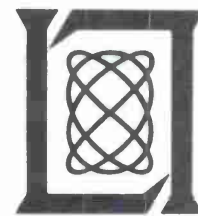
Issued 13 January 1970

Prepared under Electronic Systems Division Contract AF 19(628)-5167 by

Lincoln Laboratory

MASSACHUSETTS INSTITUTE OF TECHNOLOGY

Lexington, Massachusetts



This document has been approved for public release and sale; its distribution is unlimited.

The work reported in this document was performed at Lincoln Laboratory, a center for research operated by Massachusetts Institute of Technology, with the support of the Department of the Air Force under Contract AF 19(628)-5167.

This report may be reproduced to satisfy needs of U.S. Government agencies.

Non-Lincoln Recipients

PLEASE DO NOT RETURN

Permission is given to destroy this document
when it is no longer needed.

ABSTRACT

This report covers in detail the solid state research work at Lincoln Laboratory for the period 1 August through 31 October 1969. The topics covered are Solid State Device Research, Materials Research, and Physics of Solids.

Accepted for the Air Force
Franklin C. Hudson
Chief, Lincoln Laboratory Office

INTRODUCTION

I. SOLID STATE DEVICE RESEARCH

Far infrared radiation corresponding to transitions of impact ionized electrons from excited-donor and conduction-band states to the ground state of a shallow donor has been observed in high-purity epitaxial layers of GaAs at 4.2°K. The emission has a main peak at $282\ \mu$ (4.4 meV) due to transitions from the lowest excited-donor state to the ground state and a broad continuum extending to higher photon energies. A total radiated power of 10^{-7} W has been observed, corresponding to an external efficiency of about 10^{-6} .

Proton bombardment has been used to produce n-type layers in p-type InSb and to fabricate high-quality n-p junction photovoltaic detectors. The 20-mil-diameter diodes produced in this manner have shown incremental resistances at zero bias in the range of several hundred thousand ohms. A peak detectivity of $7.7 \times 10^{10}\ \text{cm}\sqrt{\text{Hz}}/\text{W}$ has been observed at $5.3\ \mu$, which is about half the background limited value for this wavelength. An array of 12 diodes has been fabricated on a single InSb wafer using this method; all diodes had 500°K black body detectivities in excess of $1 \times 10^{10}\ \text{cm}\sqrt{\text{Hz}}/\text{W}$.

The temperature and magnetic field dependence of the Hall coefficient factor for polar optical mode scattering have been measured in high-purity n-type epitaxial layers of GaAs between 77° and 300°K in magnetic fields up to 90 kG. The experimental variation is in fair agreement with theoretical calculations and provides the first test for the theory. This variation produces a change in the measured Hall constant in high-purity GaAs which can give the appearance of a higher calculated carrier concentration at 77°K than at 300°K.

The conductivity of the ferromagnetic semiconductor EuO has been measured as a function of temperature from 30° to 300°K in magnetic fields up to 50 kG. The resistivity exhibits a sharp increase by as much as 10^8 between 50° and 70°K. Data are interpreted in terms of a transfer of electrons between a conduction band whose energy position is a strong function of temperature and magnetic field and a trap whose energy is roughly constant.

II. MATERIALS RESEARCH

An ideal equation for the relationship between liquidus and solidus compositions has been used to calculate solidus curves for a large number of homogeneous, monotonic alloy systems from liquidus and enthalpy of fusion data. The calculated curves are in good to excellent agreement with published solidus data, except for a few systems where re-evaluation of the experimental data is indicated.

The solidus curve of the pseudobinary CdTe-ZnTe system has been determined by differential thermal analysis of heating curves obtained in experiments on homogenized alloys. Because of the relatively narrow liquidus-solidus gap, it has been possible to grow single crystals of the alloys by the Bridgman method from stoichiometric melts.

A large number of tellurates based on the alkali antimonates NaSbO_3 and LiSbO_3 have been prepared by sintering stoichiometric mixtures of oxides and carbonates. Most of these compounds have either the ilmenite structure of NaSbO_3 or the LiSbO_3 structure, but $\text{Na}_2\text{MnTeO}_6$, $\text{Na}_2\text{SnTeO}_6$, and the high-temperature form of $\text{Na}_2\text{GeTeO}_6$ have a hexagonal structure which has not been identified.

Two spinels, Co_2RuO_4 and ZnCoRuO_4 , have been prepared by reacting Co and Zn carbonates with Ru metal. These are the first reported spinels containing Ru^{4+} .

Quantitative treatment of x-ray powder diffraction data has shown that tetragonal $\alpha\text{-VOSO}_4$ has the same structure as NbOPO_4 . The magnetic properties of this tetragonal form differ markedly from those of the orthorhombic $\beta\text{-VOSO}_4$.

An earlier study of chemical analysis by EDTA titrations using color change end points showed that Zn can be determined to a precision of two parts per thousand by an automatic photometric method. It has been found that for many other metals comparable precision can be obtained by manual photometric titration, but not by the automatic method.

The published technique for making mass spectrographic analyses on frozen aqueous solutions has been modified by replacing the graphite sample cup and counterelectrode with a nickel sample cup and platinum counterelectrode. Initial results indicate that the modified method should make it possible to determine almost all elements in solution at the level of ten parts per million (atomic) or higher.

III. PHYSICS OF SOLIDS

The study of interband magnetoreflexion from $\alpha\text{-Sn}$ has been completed. Possible explanations for the systematic deviation at high photon energies of the theory based on the inverted band structure model have been proposed.

Extension of the low-temperature stress measurements on phosphorus-doped silicon to more homogeneous and higher stresses (up to 17.5×10^8 dynes/cm²), about three times that of earlier experiments, has resulted in a significant improvement in the impurity optical spectra. This has allowed the observation of a nonlinear energy shift of the transition energies, which is explained theoretically by the downward shift of the ground state with stress.

A discrepancy exists between the observed deformation potential for donors in silicon obtained in photoexcitation spectra and hyperfine interaction measurements. The possibility of explaining the difference by considering a dipolar hyperfine interaction was explored and shown to be unlikely.

Shubnikov-de Haas measurements under hydrostatic pressure (up to 8 kbars) have been carried out in $\text{Pb}_{1-x}\text{Sn}_x\text{Te}$ alloys of composition $0.16 \leq x \leq 0.32$. The shape of the Fermi surface appears not to change with pressure although there is a decrease of the cyclotron effective masses.

Previous optical reflectance studies of magnetic ordering effects in the magnetic semiconductors EuS and EuSe , which have provided evidence that the conduction band is spin-polarized in

Introduction

the ferromagnetic state and that the low-energy peak E_1 (at ~ 1.5 eV) is due to $4f^7 \rightarrow 4f^6 5d(t_{2g})$ transitions, have now been extended to the higher energy peak, E_2 (at ~ 4 eV). The results suggest that the E_2 peak is due at least in part to $4f^7 \rightarrow 4f^6 5d(e_g)$ transitions. Similar measurements have also been made on EuTe which is antiferromagnetic below 10°K. In this case, the reflectance is strongly field dependent at the lower fields. At high fields (above 60 kOe), the E_1 structure has a form identical to that of ferromagnetic EuO, EuS and EuSe, and this is taken as evidence for field-induced spin alignment in EuTe.

Various aspects of neutron diffraction experiments yield conflicting results as to the order of the ferrimagnetic-antiferromagnetic transition in Cr_5S_6 . In order to resolve this apparent contradiction, Cr_5S_6 is being examined theoretically by means of the Heisenberg Hamiltonian, and experimentally by investigating its magnetic properties as a function of pressure as well as magnetic field and temperature.

Accurate measurements of spin-wave resonance absorption peaks on two permalloy films from 5 to 70 GHz show that the deviation from a $1/p^2$ fall-off is a strong function of frequency. Consequently, any intensity model must incorporate such a frequency dependence. Furthermore, the spin-wave dispersion was quadratic in mode number from $p = 9$ to 21; also the mode number assignment for these films was unambiguous.

A new type of single determinant variational approach has been applied to a Hubbard model of localized and band magnetic semiconductors. Stability boundaries for different phases of the system, based on free energy, have been obtained.

A mathematical criterion for a phase transition, based on the asymptotic degeneracy of the largest eigenvalue of a certain linear operator, has been applied to the exactly soluble case of a linear chain of classical spins of arbitrary dimension interacting through an isotropic Heisenberg Hamiltonian.

The two-magnon spectrum of KNiF_3 has been observed and compared with the Green's function calculation of the line shape for $s = 1$ spins. Agreement between the calculated and observed line shape is excellent.

The study of laser scattering from α -quartz has been continued. A linear wavevector dispersion, previously reported for the optical phonon, has now been observed in the transverse acoustic branches via backward Brillouin scattering.

CONTENTS

Abstract	iii
Introduction	iv
Organization	viii
Reports by Authors Engaged in Solid State Research	ix
 I. SOLID STATE DEVICE RESEARCH	 1
A. Far Infrared Recombination Radiation from Impact Ionized Shallow Donors in GaAs	1
B. p-n Junction Photodetector in InSb Fabricated by Proton Bombardment	3
C. Variation of Hall Constant Between 300° and 77°K in High-Purity GaAs	7
D. Temperature and Magnetic-Field Dependence of Conductivity of EuO	8
 II. MATERIALS RESEARCH	 13
A. Calculation of the Liquidus-Solidus Gap in Homogeneous, Monotonic Alloy Systems	13
B. Solidus Curve and Crystal Growth of CdTe-ZnTe Alloys	13
C. Preparation of Tellurates Based on NaSbO ₃ and LiSbO ₃	16
D. Preparation and Magnetic Properties of Ruthenium Spinel	18
E. Structure and Magnetic Properties of VOSO ₄	18
F. Chemical Analysis by Photometric EDTA Titrations	26
G. Mass Spectrographic Analysis of Frozen Aqueous Solutions	26
 III. PHYSICS OF SOLIDS	 29
A. Electronic Band Structure	29
B. Magnetism	35
C. Laser Scattering	43

ORGANIZATION

SOLID STATE DIVISION

A. L. McWhorter, *Head*
 P. E. Tannenwald, *Associate Head*
 M. J. Hudson, *Assistant*
 E. P. Warekois
 C. R. Grant

SOLID STATE THEORY

H. J. Zeiger, *Leader*
 M. M. Litvak, *Assistant Leader*

Bari, R. A.	Landon, S. N.
Brine, N. S.	Larsen, D. M.
Chinn, S. R.*	Ngai, K. L.
Davies, R. W.	Palm, B. J.†
Dresselhaus, G. F.	Wilson, A. R. M.
Kaplan, T. A.	Young, C. Y.
Kleiner, W. H.	

SOLID STATE PHYSICS

J. G. Mavroides, *Leader*
 G. B. Wright, *Assistant Leader*

Adler, D.‡	Henrich, V. E.
Allen, J. W.	Johnson, E. J.
Bajorek, C. H.‡	Kernan, W. C.
Barch, W. E.	Kolesar, D. F.
Blum, F. A., Jr.	Krag, W. E.
Brandt, R. C.	Melngailis, J.
Burke, J. W.	Menyuk, N.
Crooker, P. P.	Nill, K. W.
DeFeo, W. E.	Parker, C. D.
Dresselhaus, M. S.†	Pine, A. S.
Dwight, K., Jr.	Scouler, W. J.
Feinleib, J.	Waldman, J.*
Feldman, B.	Weber, R.
Groves, S. H.	

ELECTRONIC MATERIALS

J. B. Goodenough, *Leader*
 A. J. Strauss, *Associate Leader*

Anderson, C. H., Jr.	Longo, J. M.
Arnott, R. J.	Mastromattei, E. L.
Banus, M. D.	O'Connor, J. R.
Batson, D. A.	Owens, E. B.
Brebrick, R. F., Jr.	Pierce, J. W.
Button, M. J.	Plonko, M. C.
Capes, R. N., Jr.	Racchah, P. M.
Delaney, E. J.	Reed, T. B.
England, R. E.	Roddy, J. T.
Fahey, R. E.	Searles, I. H.
Finn, M. C.	Smith, F. T. J.
Iseler, G. W.	Stack, T. E.
Kafalas, J. A.	Steininger, J. M.
Kasper, H. M.	Temkin, R. J.*
LaFleur, W. J.	Wheatley, G. E.
Lavine, M. C.†	

APPLIED PHYSICS

J. O. Dimmock, *Leader*
 T. C. Harman, *Assistant Leader*
 I. Melngailis, *Assistant Leader*

Brueck, S. R. J.*	Mroczkowski, J.†
Calawa, A. R.	Murphy, R. A.*
Carter, F. B.	Oliver, M. R.*
Caswell, F. H.	Orphanos, W. G.
Clough, T. F.	Paladino, A. E.
Donnelly, J. P.	Rossi, J. A.
Ferrante, G. A.	Spears, D. L.
Foyt, A. G.	Stillman, G. E.
Hurwitz, C. E.	Ward, J. H. R., III
Krohn, L., Jr.	Wolfe, C. M.
Lindley, W. T.	Woods, R. J.
Mooradian, A.	Youtz, P.

* Research Assistant

† Part Time

‡ Summer Staff

REPORTS BY AUTHORS ENGAGED IN SOLID STATE RESEARCH

15 August through 15 November 1969

PUBLISHED REPORTS

Journal Articles*

JA No.

3301	Effective-Mass Theory for Polarons in External Fields	D. M. Larsen	Phys. Rev. <u>180</u> , 919 (1969), DDC AD-694896
3380	Partial Pressures of Zn and Te ₂ over ZnTe up to 917°C	R. F. Brebrick	J. Electrochem. Soc. <u>116</u> , 1274 (1969), DDC AD-696239
3400	Magnetoreflexion Studies in Arsenic	M. Maltz M. S. Dresselhaus	Phys. Rev. <u>182</u> , 741 (1969), DDC AD-696242
3417	Space-Time Symmetry Restrictions on Transport Coefficients. III. Thermogalvanomagnetic Coefficients	W. H. Kleiner	Phys. Rev. <u>182</u> , 705 (1969), DDC AD-695895
3441A	Magnetoreflexion Studies on the Band Structure of Bismuth-Antimony Alloys	E. J. Tichovolsky J. G. Mavroides	Solid State Commun. <u>7</u> , 927 (1969), DDC AD-693671
3442	Effects of Light on the Charge State of InSb-MOS Devices	W. E. Krag R. J. Phelan, Jr. J. O. Dimmock	J. Appl. Phys. <u>40</u> , 3661 (1969)
3449	Magnetoemission Experiments in Pb _{1-x} Sn _x Te	J. F. Butler	Solid State Commun. <u>7</u> , 909 (1969)
3467	Absolute Experimental X-Ray Form Factor of Aluminum	P. M. Raccach V. E. Henrich	Phys. Rev. <u>184</u> , 607 (1969)
3468	Magneto spectroscopy of Shallow Donors in GaAs	G. E. Stillman C. M. Wolfe J. O. Dimmock	Solid State Commun. <u>7</u> , 921 (1969), DDC AD-693903
3490	Hydroxyl and Water Masers in Protostars	M. M. Litvak	Science <u>165</u> , 855 (1969), DDC AD-696247
3491	Perturbation of the Refractive Index of Absorbing Media by a Pulsed Laser Beam	P. R. Longaker M. M. Litvak	J. Appl. Phys. <u>40</u> , 4033 (1969)

* Reprints available.

Reports

JA No.

- | | | | |
|-------|---|--|--|
| 3503A | Millimetre Wave Emission by Interstellar Dust | M.M. Litvak | Nature <u>223</u> , 1143 (1969) |
| 3547 | Polaron Cyclotron Resonance in CdTe | J. Waldman
D.M. Larsen
P.E. Tannenwald
C.C. Bradley*
D.R. Cohn*
B. Lax* | Phys. Rev. Letters <u>23</u> , 1033 (1969) |
| 3583 | Far Infrared Recombination Radiation from Impact Ionized Shallow Donors in GaAs | I. Melngailis
G.E. Stillman
J.O. Dimmock
C.M. Wolfe | Phys. Rev. Letters <u>23</u> , 1111 (1969) |

MS No.

- | | | | |
|-------|--|---|---|
| 2024 | The Raman Spectrum of Trigonal, α -Monoclinic and Amorphous Selenium | A. Mooradian
G.B. Wright | <u>The Physics of Selenium and Tellurium</u> (Pergamon, New York, 1969), DDC AD-694135 |
| 2166A | Electronic Raman Scattering from Impurities in Semiconductors | G.B. Wright
A. Mooradian | } <u>Proc. 9th International Conference on Physics of Semiconductors</u> , Vol. 2 (Nauka, Moscow, 1968) |
| 2194 | The Two-Phonon Infrared and Raman Spectrum of CdTe | A. Mooradian
G.B. Wright | |
| 2236 | Raman Scattering from Magneto-plasma Waves in Semiconductors | A.L. McWhorter
P.N. Argyres | |
| 2183 | Interband Magnetoreflexion of Gray Tin | S.H. Groves
C.R. Pidgeon*
A.W. Ewald*
R.J. Wagner* | } <u>Proc. 9th International Conference on Physics of Semiconductors</u> , Vol. 1 (Nauka, Moscow, 1968) |
| 2188 | Electroreflection Study of Inversion Asymmetry and Warping Induced Interband Magneto-Optical Transitions in InSb | C.R. Pidgeon*
S.H. Groves | |
| 2195 | An Exciton in a High Magnetic Field - Germanium | E.J. Johnson | |
| 2236A | Raman Scattering from Magneto-plasma Waves in Semiconductors | A.L. McWhorter
P.N. Argyres | <u>Light Scattering Spectra of Solids</u> , G.B. Wright, ed. (Springer-Verlag, New York, 1969), DDC AD-695132 |
| 2331 | Raman Scattering from Spin-Density Fluctuations in n-GaAs | D.C. Hamilton
A.L. McWhorter | <u>Light Scattering Spectra of Solids</u> , G.B. Wright, ed. (Springer-Verlag, New York, 1969), DDC AD-695754 |
| 2332 | Light Scattering from Single-Particle Electron and Hole Excitations in Semiconductors | A. Mooradian | <u>Light Scattering Spectra of Solids</u> , G.B. Wright, ed. (Springer-Verlag, New York, 1969), DDC AD-695887 |

* Author not at Lincoln Laboratory.

MS No.

2335	Light Scattering from Plasmons and Phonons in GaAs	A. Mooradian A. L. McWhorter	<u>Light Scattering Spectra of Solids</u> , G. B. Wright, ed. (Springer-Verlag, New York, 1969), DDC AD-695752
2336	Light Scattering from Plasmons in Semiconductors	A. L. McWhorter	<u>Electronic Structures in Solids</u> (Plenum, New York, 1969), DDC AD-693902
2338	Meaning of an Anomaly in the X-Ray Scattering of ZnSe	P. M. Raccach	<u>Electronic Structures in Solids</u> (Plenum, New York, 1969), DDC AD-694134
2339	Band Approach to the Transition Metal Oxides	J. Feinleib	<u>Electronic Structures in Solids</u> (Plenum, New York, 1969), DDC AD-694133
2528	Light Scattering in Semi-conductors	A. Mooradian	<u>Festkörperprobleme IX</u> (Pergamon, New York, 1969)

UNPUBLISHED REPORTS

Journal Articles

JA No.

3499	Infrared Cyclotron Resonance and Related Experiments in the Conduction Band of InSb	E. J. Johnson D. H. Dickey	Accepted by Phys. Rev.
3501	Evidence for a Native Donor in ZnSe from High Temperature Electrical Measurements	F. T. J. Smith	Accepted by Solid State Commun.
3517	Resonant Raman Scattering from LO Phonons in Polar Semiconductors	D. C. Hamilton	Accepted by Phys. Rev.
3520	An On-Line Data Recording System	W. Krag N. Daggett R. N. Davis F. Perkins*	Accepted by Rev. Sci. Instr.
3521	Ionized Impurity Density in n-Type GaAs	C. M. Wolfe G. E. Stillman J. O. Dimmock	Accepted by J. Appl. Phys.
3524	Inelastic Light Scattering from Semiconductor Plasmas in a Magnetic Field	F. A. Blum	Accepted by Phys. Rev.
3525	Magnetic Ordering Effects in the Ultraviolet Reflectance of EuS and EuSe	W. J. Scouler J. Feinleib J. O. Dimmock C. R. Pidgeon*	Accepted by Solid State Commun.

* Author not at Lincoln Laboratory.

Reports

JA No.

3528	Linear Wavevector Shifts in the Raman Spectrum of α -Quartz and Infrared Optical Activity	A. S. Pine G. F. Dresselhaus	Accepted by Phys. Rev.
3545	Cadmium Rhenium (V) Oxide, $\text{Cd}_2\text{Re}_2\text{O}_7$	J. M. Longo P. C. Donohue* D. A. Batson	Accepted by Inorg. Synth.
3546	Transport Equation for a Fermi System in Random-Scattering Centers. II. Independent Electrons in an Arbitrarily Varying Electric Field and Strong Single-Center Potentials	J. L. Sigel P. N. Argyres*	Accepted by Phys. Rev.
3553	MIS Electroluminescent Diodes in ZnTe	J. P. Donnelly A. G. Foyt W. T. Lindley G. W. Iseler	Accepted by Solid-State Electron.
3580	Electrically Active Point Defects in Cadmium Telluride	F. T. J. Smith	Accepted by Trans. Met. Soc. AIME
3582	Interpretation of $\text{M}_x\text{V}_2\text{O}_5$ - β and $\text{M}_x\text{V}_{2-y}\text{T}_y\text{O}_5$ - β Phases	J. B. Goodenough	Accepted by J. Solid State Chem.
3585	Residual Impurities in High-Purity Epitaxial GaAs	C. M. Wolfe G. E. Stillman E. B. Owens	Accepted by J. Electrochem. Soc.
3591	Comparison of Theoretical and Experimental Charge Densities for C, Si, Ge, and ZnSe	P. M. Raccah R. N. Euwema* D. J. Stukel* T. C. Collins*	Accepted by Phys. Rev.
3592	Structure and Magnetic Properties of VO_4	J. M. Longo R. J. Arnott	Accepted by J. Solid State Chem.
3597	The Hubbard Model: Insulator or Conductor for Narrow Band Regime?	R. A. Bari R. V. Lange*	Accepted by Phys. Letters
3601	Structure of the $\text{M}_x\text{V}_2\text{O}_5$ - β and $\text{M}_x\text{V}_{2-y}\text{T}_y\text{O}_5$ - β Phases	J. Galy* J. Darriet* A. Casalot* J. B. Goodenough	Accepted by J. Solid State Chem.
MS-2666	Magnetic and Optical Properties of the High and Low Pressure Forms of CsCoF_3	J. M. Longo J. A. Kafalas J. R. O'Connor J. B. Goodenough	Accepted by J. Appl. Phys.

* Author not at Lincoln Laboratory.

Meeting Speeches*

MS No.

2545A	High Pressure Phases with Perovskite Related Structure in the System $\text{Sr}_{1+x}\text{IrO}_{3+x}$ ($x = 0, 1/3, 1/2, 1$)	J. M. Longo J. A. Kafalas	22nd International Congress on Pure and Applied Chemistry, Sydney, Australia, 20-27 August 1969
2548	Absolute Measurement of the Atomic Form-Factor of Ni	P. M. Raccach V. E. Henrich	8th International Congress on Crystallography, State University of New York, Stonybrook, 13-21 August 1969
2571A	Ion Implantation in Compound Semiconductors	A. G. Foyt	Seminar, Itek Corp., Lexington, Massachusetts, 24 September 1969
2586	Electrically Active Point Defects in Cadmium Telluride	F. T. J. Smith	Defects in Electronic Materials for Devices, Boston, 24-27 August 1969
2591	Photoluminescence due to Isoelectronic Te Traps in $\text{CdS}_{1-x}\text{Se}_x$ and $\text{Zn}_{1-y}\text{Cd}_y\text{Se}$ Alloys	G. W. Iseler A. J. Strauss	International Conference on Luminescence, University of Delaware, 25-29 August 1969
2615	Magneto-Optics	J. G. Mavroides	Conference on High Magnetic Fields and Their Applications, University of Nottingham, England, 17-19 September 1969
2617A	One-Electron Theory of Interband Transitions	G. Dresselhaus	Seminar, General Electric Research and Development Center, Schenectady, 7 October 1969
2620	Thermodynamic Behavior and Deviations from Stoichiometry	R. F. Brebrick	136th National Meeting, Electrochemical Society, Inc., Detroit, 5-10 October 1969
2621	Variations of Infrared Cyclotron Resonance and the Density of States Near the Conduction Band Edge of InSb	E. J. Johnson D. H. Dickey	3rd Materials Research Symposium, Electron Density of States, Gaithersburg, Maryland, 3-6 November 1969
2628	On the Optical Properties and the Density of States in Arsenic	R. W. Brodersen† M. S. Dresselhaus	
2630	Optical Properties of Aluminum	G. Dresselhaus M. S. Dresselhaus D. Beaglehole†	
2631	Localized States in Narrow Band and Amorphous Semiconductors	D. Adler J. Feinleib	

* Titles of Meeting Speeches are listed for information only. No copies are available for distribution.

† Author not at Lincoln Laboratory.

Reports

MS No.

2623	Laser Beam Trapping and Non-Linear Interactions in Semi-conductors	A. Mooradian	NEREM-69, Boston, 5-7 November 1969
2632	Explanation of Cyclotron Resonance in Finite Slab Galt Geometry	A. R. Wilson	Fundamental Problems in Metals Conference, Banff, Alberta, Canada, 11-22 August 1969
2644	Linear Wavevector Dispersion of the Shear Wave Phase Velocity in α -Quartz	A. S. Pine	Conference on Interaction of Light with Sound Waves, San Diego, 4-5 November 1969
2681	Optical Reflectance Study of the Magnetic Ordering Effects in EuO, EuS, EuSe and EuTe	C. R. Pidgeon* J. Feinleib W. J. Scouler	Symposium on Magnetic Semi-conductors, Yorktown Heights, New York, 13-14 November 1969
2683	Temperature and Magnetic Field Dependence of the Conductivity of EuO	M. R. Oliver J. O. Dimmock T. B. Reed	
2708	Optical Properties of the Europium Chalcogenides	J. O. Dimmock	
2684	A Conceptual Phase Diagram for Outer Electrons in Solids	J. Goodenough	Seminar, 3-M Company, St. Paul, Minnesota, 17 October 1969
2691	Band Structure of Rare Earth Metals	J. O. Dimmock	The Metallurgical Society Fall Meeting, Philadelphia, 13-16 October 1969
2693	Comparison of Absolute X-Ray Form-Factors with the Predictions of Band Calculations	P. M. Raccach	Seminar, Purdue University, 9 October 1969
2694	Mass Spectrometry	E. B. Owens	Seminar, Instrumentation Laboratory, Lexington, Massachusetts, 13 November 1969
2696	Infrared Studies in Small Bandgap Pb-Sn Salt Materials	A. R. Calawa	Seminar, Case Institute of Technology, 7 October 1969
2705	Interstellar Molecules and Non-Equilibrium Processes	M. M. Litvak	Physics Colloquium, University of Maryland, 29 October 1969
2706	The Effects of Light on the Charge State of InSb MOS Structures	W. E. Krag	Seminar, University of Rhode Island, 22 October 1969
2718	Inelastic Light Scattering from Semiconductor Plasmas in a Magnetic Field	F. A. Blum	Seminar, Yale University, 6 November 1969

* Author not at Lincoln Laboratory.

MS No.

2720	Spectroscopy of Shallow Donor Levels in GaAs Extrinsic Photodetectors	G. E. Stillman	Seminar, RCA Laboratories, Princeton, New Jersey, 6 November 1969
2726	Theory of Surface Plasmon Excitation in Low Energy Electron Diffraction and in Photoemission	K. L. Ngai	Seminar, University of Chicago, 29 October 1969
2727	Theory of Antiferromagnetism and Ferrimagnetism	J. B. Goodenough	Ceramics Research Meeting, University of Florida, 12 November 1969
2729	Two-Magnon Raman Scattering from Magnetic Insulators	S. R. Chinn	Seminar, M.I.T., 7 November 1969
2730	Non-Equilibrium Processes Related to Interstellar Molecules	M. M. Litvak	Course on Radio Spectral Lines, Harvard College Observatory, 4 November 1969

I. SOLID STATE DEVICE RESEARCH

A. FAR INFRARED RECOMBINATION RADIATION FROM IMPACT IONIZED SHALLOW DONORS IN GaAs

Radiation corresponding to transitions from excited-shallow-donor and conduction-band states to the donor ground state has been observed in impact ionized GaAs at temperatures near 4.2°K. Spectral measurements show a main peak at a wavelength of 282μ (4.4 meV) corresponding to a $2p \rightarrow 1s$ transition and a broader continuum extending to higher photon energies. A total radiated power of 10^{-7} W has been measured corresponding to an external quantum efficiency of about 10^{-6} .

The high-purity epitaxially grown GaAs samples used were similar to those studied in photoconductivity experiments.^{1,2} Most of the measurements were made on a 0.4-mm thick epitaxial layer grown on a semi-insulating substrate. For this sample, a shallow-donor concentration of $N_D = 2.5 \times 10^{14} \text{ cm}^{-3}$ and a total acceptor concentration of $N_A = 1.6 \times 10^{14} \text{ cm}^{-3}$ were determined from an analysis of the temperature dependence of the Hall constant using the usual single-donor statistics. Ohmic contacts were made by alloying Sn along the two longer edges of the 5×6 -mm sample. The sample was mounted in a gold-plated stainless-steel light pipe which was immersed in liquid helium.

At 4.2°K, the conduction electrons in the GaAs sample are frozen out on the shallow impurity states which have a measured thermal ionization energy of about 5 meV. When a small critical voltage (1.8 V for the 5-mm long sample used) is applied, the carriers are released by impact ionization.³ Following breakdown, the voltage generally drops to a lower value (1.1 V) and the current then increases by about six orders of magnitude at a nearly constant voltage as the number of carriers in the sample increases. When nearly all the donors are ionized, the sample conductance approaches a limiting value. From previous studies of impact ionization in germanium,⁴ the initial breakdown is expected to occur in a filament which grows laterally as the current is increased.

Two methods were used to measure the radiation. In the first experiment, the GaAs emitter was mounted in the same light pipe with an InSb detector which was positioned in a 30-kG solenoidal superconducting magnet. The emitter was outside the magnet. Since the InSb photoconductivity peak shifts to shorter wavelengths as the magnetic field is increased,⁵ the InSb detector can be used as a crude far infrared spectrometer. In a second experiment, spectral measurements with a resolution of about 0.15 meV were made using a Michelson interferometer and a GaAs photoconductive detector. The epitaxial GaAs detector was mounted in liquid helium in a separate dewar. Its peak detectivity was two orders of magnitude greater than that of the InSb detector; however, it had a long wavelength cutoff at about 300μ . In both experiments, the emitter was pulse-biased at a repetition rate between 260 Hz and 1 kHz and a duty cycle between 1/10 and 1/2. The detector output was measured with a lock-in amplifier.

Data obtained with the magnetically tuned InSb detector showed a single broad peak near 5 meV (250μ). Figure I-1 shows the emission spectrum obtained using the interferometer and a GaAs detector. The general shape of the emission spectrum resembles the photoconductivity

Section I

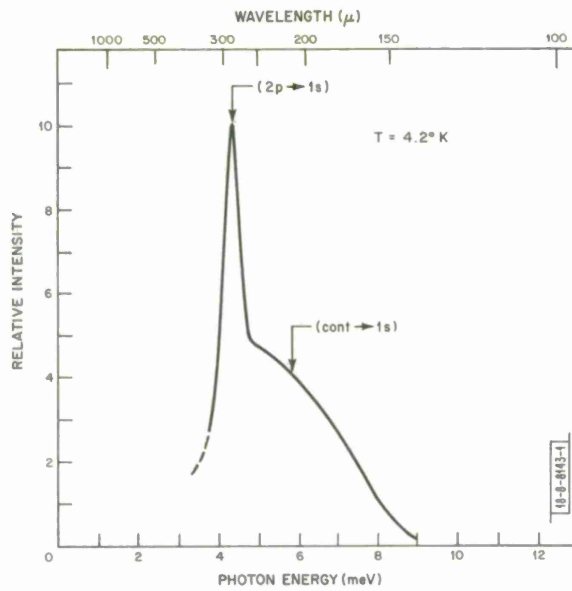
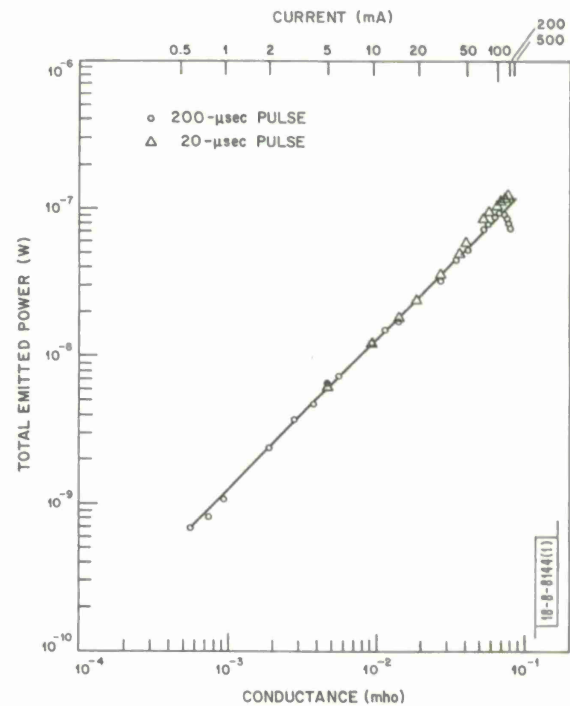


Fig. 1-1. Radiation spectrum of impact ionized GaAs sample at 4.2°K biased with 260-μsec long 100-mA pulses at 1-kHz repetition rate.

Fig. 1-2. Dependence of total radiated power on conductance of impact ionized GaAs sample at 4.2°K. Current pulses 200- and 20-μsec long were applied at 1.5-kHz repetition rate.



spectra obtained on similar GaAs samples.¹ The narrow peak at 4.4 meV (282 μ) coincides in photon energy with the main photoconductivity peak which was clearly identified with a transition from the 1s ground state to the 2p excited state of the donor. Emission from the higher excited impurity states is broadened and merges with that from the continuum. The identification of the main emission peak was confirmed by Zeeman splitting of the 2p \rightarrow 1s line which was observed when the emitter was placed in a 7.5-kG magnetic field. Spacing of the magnetic levels agreed with that observed for the 1s \rightarrow 2p line in the photoconductivity spectrum.¹

Transitions from conduction-band states are expected at energies higher than the calculated donor ionization energy¹ of 5.86 meV indicated by an arrow in Fig. I-1. The high-energy tail of the spectrum, which extends about 3 meV to the right of the arrow in the figure, can be attributed to hot electron recombination. The energy of some of the electrons is expected to extend beyond the 5.86-meV donor ionization energy, which is the approximate minimum energy needed by a conduction-band electron for impact ionization.

Measurements of the radiated power were made by coupling the emitted radiation directly to the GaAs detector. The variation of the total power with emitter conductance is shown in Fig. I-2. At the higher currents, 20- μ sec pulses were used in the emitter to avoid heating which causes a decrease in emitted power with the 200- μ sec pulses at currents beyond 50 mA. The nearly linear dependence of the radiated power on sample conductance seen in Fig. I-2 is expected if a constant fraction of the ionized carriers recombine radiatively (constant quantum efficiency) and if the mobility is independent of current.

A lower limit for the response speed of the emitter was obtained by observing the radiation pulses directly with an oscilloscope. A rise and fall time of 2 μ sec was measured which was limited by the RC constant of the detector circuit.

The radiative lifetime for the transition of free carriers to the 1s state, estimated from corresponding calculations for the hydrogen atom,⁶ has a value of 3.6×10^{-4} sec. For the 2p \rightarrow 1s transition, the radiative lifetime has a calculated value of 1.7×10^{-4} sec. From measurements of the conductivity decay times following pulse excitation, we can estimate a lifetime for conduction band electrons of about 7×10^{-9} sec, which is much shorter than the calculated radiative lifetimes, indicating that the recombination is predominantly nonradiative.

The quantum efficiency for direct radiative recombination of conduction-band electrons predicted from the ratio of the estimated carrier lifetime to the calculated radiative lifetime is about 2×10^{-5} . From the highest measured radiated power of 1.3×10^{-7} W, we estimate an external quantum efficiency of 1×10^{-6} by taking the ratio of the number of photons detected per second to the number of electrons recombining per second in the sample, which was obtained assuming that all of the donors are ionized ($n = 0.9 \times 10^{14}$ cm⁻³), and that the electron lifetime is 7×10^{-9} sec. The power efficiency, which is constant at currents up to nearly 30 mA, is 1.2×10^{-6} , very close to the estimated quantum efficiency.

I. Melngailis J. O. Dimmock
G. E. Stillman C. M. Wolfe

B. p-n JUNCTION PHOTODETECTOR IN InSb FABRICATED BY PROTON BOMBARDMENT

We have found that proton bombardment can be used to produce n-type layers in p-type InSb, and have used this technique to fabricate high-quality n-p junction photovoltaic detectors. In

Section I

this section, we shall describe the bombardment procedure and device fabrication, and present electrical and photovoltaic measurements on the diodes.

The samples were prepared from p-type InSb slices which had a nominal carrier concentration of $5 \times 10^{15}/\text{cm}^3$ at 77°K. Each slice was etched for 30 sec in a 20-percent solution of bromine in methanol, and subsequently rinsed in methanol. The sample was then coated with 1500 Å of pyrolytic SiO₂ deposited at 340°C from the reaction of silane and oxygen. Each sample was bombarded with a monoenergetic beam of protons, with the sample at room temperature. For a typical bombardment, the proton energy was 100 keV, with a beam current density of $0.03 \mu\text{A}/\text{cm}^2$, and a total proton dose of $10^{14}/\text{cm}^2$. As an initial check on the electrical properties of the bombarded layer, van der Pauw Hall-effect measurements were done on samples prepared as above. Following bombardment, four gold contacts were plated onto the top surface, through holes in the SiO₂, and a cloverleaf pattern etched around these contacts. At 77°K, the current-voltage characteristics between these contacts were linear, whereas diode characteristics with low leakage current were observed between the pattern and an ohmic contact on the substrate. Because of this diode isolation, it was possible to make the van der Pauw measurements on the bombarded layer at 77°K. These measurements showed that the layer was n-type. It had a sheet carrier concentration of $10^{13}/\text{cm}^2$, and an electron mobility of $15,000 \text{ cm}^2/\text{V sec}$. The average carrier concentration in the bombarded layer, which is about 1μ thick, was $10^{17}/\text{cm}^3$.

By using the bombardment to create the n-type layer, n-p junction diodes for use as photovoltaic detectors have been fabricated. The device structure is shown in Fig. I-3. Prior to

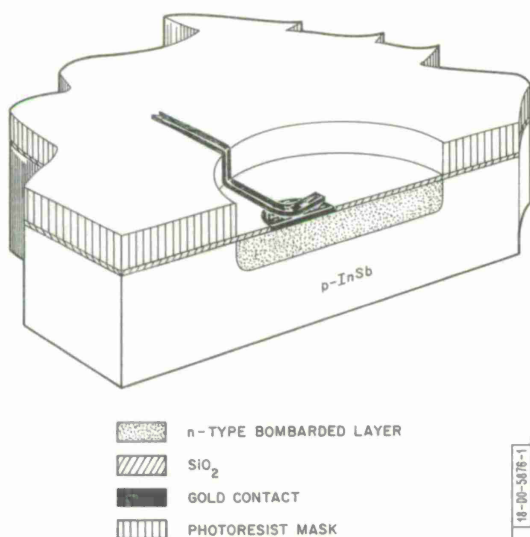


Fig. I-3. Sketch of n-p InSb junction photovoltaic detector fabricated using proton bombardment.

bombardment, the sample is coated with a 20- μ thick layer of photoresist. This layer is sufficiently thick to prevent the proton beam from reaching the sample. Consequently, only those areas from which the photoresist has been removed will be bombarded. Then, 20-mil-diameter holes are opened in the photoresist, and the sample is bombarded as above. Following bombardment, the remaining photoresist is removed and 5-mil-diameter holes are opened in the oxide layer for a contact. Gold is then plated into the 5-mil holes to provide an ohmic contact to the n-type bombarded layer. (We have found that 1000-Å thick gold contacts may be applied prior to bombardment, with no measurable effect on the diode characteristics.)

Following the gold plating, the diodes are mounted on small transistor headers and placed in liquid nitrogen vacuum dewars for electrical evaluation.

The current-voltage characteristics for one of the best diodes are shown in Fig. I-4. As may be seen, the incremental resistance of this device around zero bias is in the range of several hundred thousand ohms with incremental resistance values as large as 1 megohm for a reverse bias of 0.5 V.

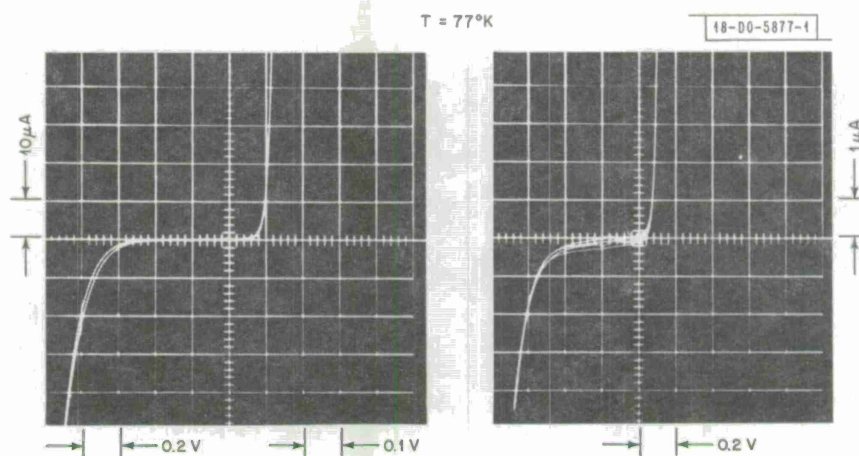


Fig. I-4. Current-voltage characteristics of n-p InSb junction diode at 77°K.

We have also measured the capacitance-voltage relation for some of these devices. A typical diode has a zero-bias capacitance of about 100 pF, and the capacitance decreases with increasing voltage as $V^{-0.43}$, suggesting that the diode has a slightly graded doping profile. The zero-bias capacitance is about the value expected for a 20-mil-diameter diode on a substrate with a carrier concentration of $5 \times 10^{15}/\text{cm}^3$.

The photovoltaic properties of these diodes were evaluated by measuring their black body detectivity and also by measuring their relative response as a function of wavelength. The black body detectivity was measured using a 500°K black body and a 900-Hz chopping frequency. The largest value measured for these diodes was $D^*(500, 900, 1) = 2 \times 10^{10} \text{ cm } \sqrt{\text{Hz}}/\text{W}$. This measurement, combined with a relative spectral response measurement, gave a calculated detectivity as a function of wavelength which is shown in Fig. I-5. As may be seen, the detectivity increases with increasing wavelength from the visible, reaching a peak at 5.3μ . The peak detectivity, $7.7 \times 10^{10} \text{ cm } \sqrt{\text{Hz}}/\text{W}$, is about half of the background-limited value for this wavelength.

These diodes have typically been fabricated as an array of twelve on a single substrate. On many of the wafers, most of the diodes have had characteristics similar to those reported above. On one wafer, all twelve diodes had black body detectivities greater than $1 \times 10^{10} \text{ cm } \sqrt{\text{Hz}}/\text{W}$.

The response speed of these diodes was measured by placing the diode in a 50-ohm coaxial system, and loading the diode with 50 ohms. The diode response to a pulsed GaAs diode laser indicated that the rise and fall times are less than 20 nsec.

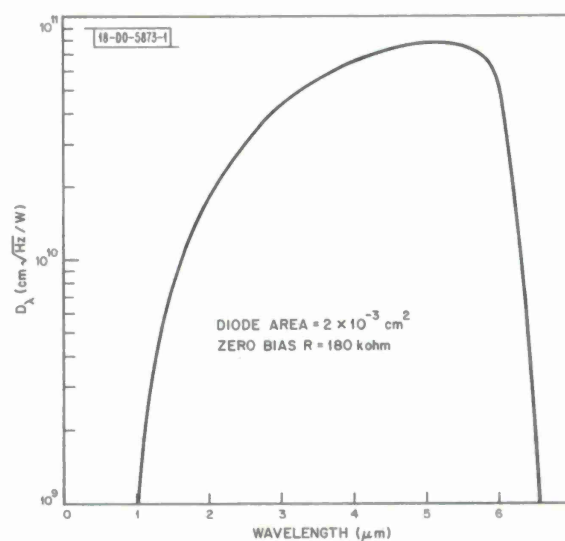


Fig. I-5. Detectivity vs wavelength for InSb photovoltaic detector at 77°K.

Section I

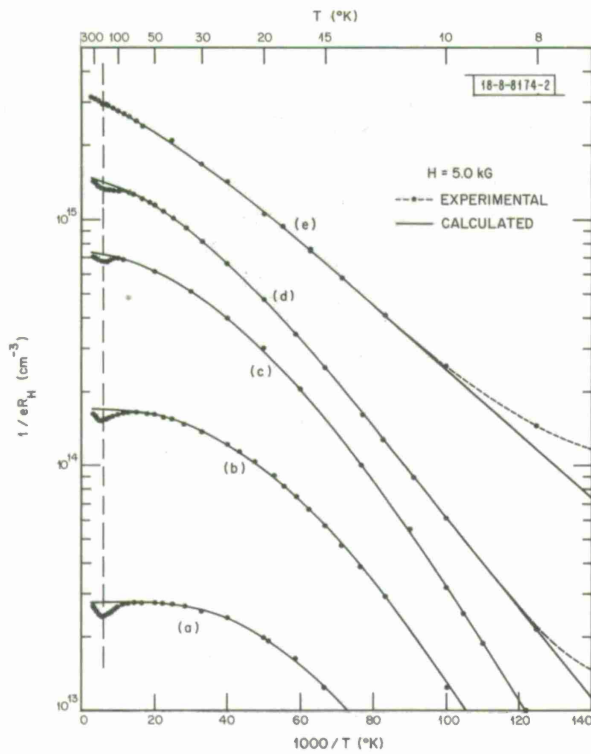


Fig. I-6. Temperature variation of $1/eR_H$ measured at 5 kG for series of samples with carrier concentrations from about 2.5×10^{13} to $3.0 \times 10^{15} \text{ cm}^{-3}$. Solid lines were calculated utilizing the usual single-donor statistics.

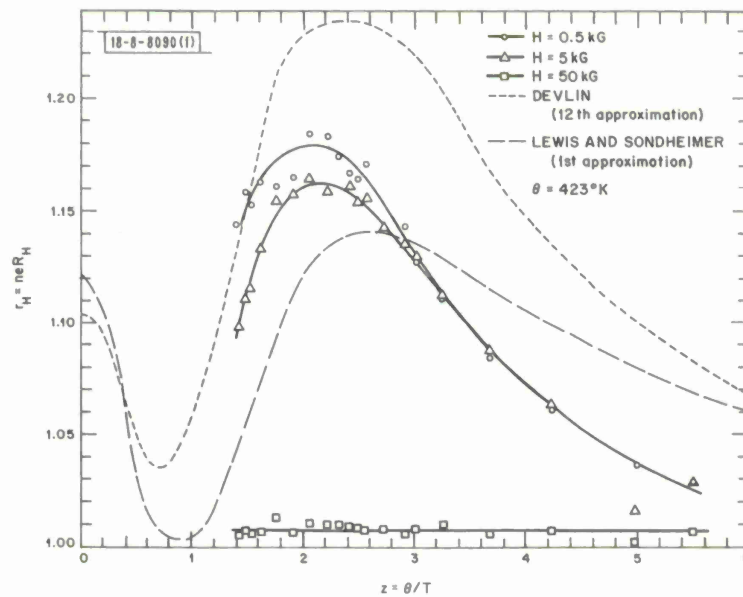


Fig. I-7. Theoretical temperature dependence of Hall factor for polar mode scattering and experimental data. Dependence is qualitatively the same. Effect disappears at 50 kG.

This technique is exciting as it is extremely difficult to fabricate n- on p-InSb diodes by diffusion, and p- on n-diodes are adversely affected by the surface state properties of InSb which tend to make the surface p-type. The n- on p-diodes fabricated by proton bombardment appear to be free from these problems.

A. G. Foyt
W. T. Lindley
J. P. Donnelly

C. VARIATION OF HALL CONSTANT BETWEEN 300° AND 77°K IN HIGH-PURITY GaAs

We have observed a temperature variation of the Hall constant in high-purity epitaxial GaAs, resulting in a calculated carrier concentration at 77°K which is higher than the calculated carrier concentration at 300°K. This anomaly in calculated carrier concentration has also been observed⁷ in other similar epitaxial GaAs samples. We present experimental data on the temperature and magnetic-field dependence of the Hall constant which indicate that this behavior is due to the temperature variation of the Hall coefficient factor for polar optical mode scattering.

Figure I-6 shows a slightly expanded version of the usual temperature variation of $1/eR_H$ (solid points and dashed curves) for samples of n-type GaAs with room-temperature carrier concentrations from about 2.5×10^{13} to $3.0 \times 10^{15} \text{ cm}^{-3}$. The solid lines were calculated using the usual single-donor statistics. At low temperatures, below about 50°K, donor deionization causes a decrease in the measured carrier concentration. However, in the high-temperature range where the carrier concentration is not expected to change, a small dip which has a minimum (indicated by the vertical dashed line) at about 170°K is observed in the experimental data. The dip becomes less pronounced as the carrier concentration becomes larger, and it is barely evident for sample (e), which has a carrier concentration of about $3 \times 10^{15} \text{ cm}^{-3}$ at room temperature. We attribute this dip to the temperature variation of the Hall factor for polar optical mode scattering.

For the purest sample [indicated by (a) in Fig. I-6], the effect is observable in the temperature range from about 77° to 300°K, and for this sample the mobility in this temperature range is limited almost entirely by polar mode scattering. The mobility for samples (b), (c), (d), and (e) is affected by a larger contribution of ionized impurity scattering, and this could mask the temperature variation of the Hall factor due to polar mode scattering. Because of this, sample (a), which has a total ionized impurity density of only $7 \times 10^{13} \text{ cm}^{-3}$, was used for subsequent measurements.

The experimental variation of the Hall factor with temperature was determined from $r_H = R_H/R_{90 \text{ kG}}$, and the results for $H = 0.5, 5,$ and 50 kG are shown in Fig. I-7, along with the theoretical variation calculated by Lewis and Sondheimer⁸ and Devlin.⁹ The Hall factor is plotted as a function of $z = \Theta/T$, where a longitudinal optical phonon temperature of $\Theta = 423^\circ \text{K}$ (Ref. 10) was used. The Hall factors measured at 0.5 and 5 kG are in qualitative agreement with both calculations, although the shape of the curves agrees more closely with Devlin's results. In the limit of high magnetic fields, the Hall factor should be independent of temperature and approximately equal to 1, and this is the case for the results at 50 kG.

Since a universal relaxation time cannot be defined for temperatures less than Θ , the usual criterion for the breakdown of low-field Hall-effect theory, $\mu B \rightarrow 1$, does not apply, and the Hall

Section I

coefficient factor is not simply a function of μB alone but is also a function of temperature. However, the variation with magnetic field of the Hall factor for polar mode scattering has also been calculated,^{8,9} and the results of Devlin's calculations for three different temperatures as well as the experimental variation of r_H for comparable temperatures are shown in Fig. I-8. There is considerable scatter in the data, but the theoretical and experimental curves are in remarkably good agreement at the higher values of μB .

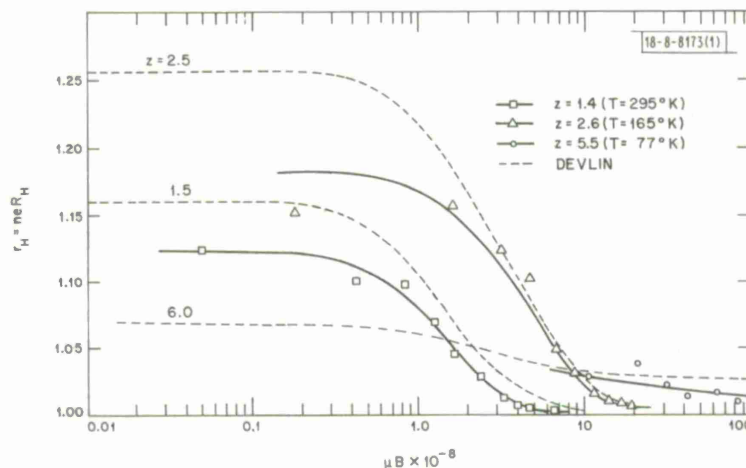


Fig. I-8. Theoretical magnetic field dependence of Hall factor for polar mode scattering and experimental data. Since a universal relaxation time for polar mode scattering cannot be defined, scattering factor does not approach 1 for same value of μB at different temperatures.

The variation of the Hall factor with degeneracy has also been calculated by Lewis and Sondheimer, and they predict a continuous decrease of r_H with increasing degeneracy at a fixed temperature. In GaAs, however, the effects of ionized impurity scattering also increase for increasing degeneracy, as previously indicated, so it is not possible to examine the variation of r_H with degeneracy alone. The disappearance of the dip in Fig. I-6 with increasing carrier concentration from sample (a) to sample (e) is probably due mainly to the increasing contribution of ionized impurity scattering, since at the temperature of the dip the Fermi energy is still 3 kT below the bottom of the conduction band for sample (e). The results of Lewis and Sondheimer predict essentially no change in the Hall factor at this degeneracy level.

G. E. Stillman
C. M. Wolfe
J. O. Dimmock

D. TEMPERATURE AND MAGNETIC-FIELD DEPENDENCE OF CONDUCTIVITY OF EuO

The conductivity of EuO has been measured as a function of temperature from 30° to 300°K in magnetic fields up to 50 kG. The zero-field resistivity exhibits a sharp elbow at about 50°K, and increases as much as 10^8 between 50° and 70°K to a broad maximum between 75° and 80°K. In an applied magnetic field, the broad maximum is rapidly decreased and the elbow is shifted

to higher temperatures. These data are interpreted in terms of a transfer of electrons between a conduction band and an electron trap. In the model, the energy separation between the band and trap level depends on the magnetic energy of the crystal and is thus a strong function of temperature and magnetic field. At low temperatures, the trap level is assumed to be above the conduction-band edge such that the electrons lie in the band. As the temperature is increased, the energy of the band edge increases such that it crosses the trap level at about 50°K. The large increase in resistivity with increasing temperature and the effects due to the magnetic field are explained by the transfer of electrons from the energy band into the trap states.

The resistivity measurements were made using the van der Pauw technique. The conducting samples were not intentionally doped and mass spectrographic analysis showed trivalent rare earth impurity concentrations in the range from 0 to 100 ppm. Annealing studies (to be reported later) have shown, however, that the conductivity can be greatly enhanced or suppressed by heating in excess Eu or in vacuum, respectively, indicating that the conductivity may be due in part to deviations from stoichiometry.

The resistivity curves of several representative samples, shown in Fig. I-9, exhibit a general pattern. At low temperatures, the resistivity rises slowly, but at about 50°K, a sharp elbow occurs in the curve and above this temperature the resistivity rises more sharply. In some samples, this rise has exceeded 10^8 . A broad peak is observed around 75° to 80°K, and the resistivity decreases gradually above this peak. There is also some structure to the curve between 60°K and the peak.

Previous infrared absorption measurements¹¹ have shown that in conducting samples the absorption coefficient for $\lambda \geq 2.5\mu$ is proportional to λ^2 , as would be expected for absorption by carriers in a conduction band. This relationship has now been established in the temperature range from 20° to 300°K, indicating the presence of band conductivity throughout this range, rather than impurity conductivity as has been proposed previously.¹² Using both the conductivity and optical absorption results, for the same sample, the electron concentration and the relaxation time can be determined assuming an effective mass. The results for one particular sample are shown in Fig. I-10 assuming $m^*/m_0 = 1$. In this sample, the free carrier absorption was too small above 54°K to be determined accurately. These results indicate that the sharp change in resistivity that commences around 50°K is primarily due to changes in carrier concentration. Whereas previous models¹² for the temperature and magnetic-field dependence of the conductivity in the Eu chalcogenides have ascribed the effects to changes in mobility, we find that the dominant effects in EuO at temperatures below T_c are due to changes in carrier concentration.

Freiser, *et al.*,¹³ and Busch and Wachter¹⁴ have shown that the energy of the optical absorption edge varies strongly with temperature, exhibiting a total increase of about 0.26 eV from $T = 0$ to about $2T_c$. Freiser, *et al.*,¹³ have related this to the spin-spin correlation function in EuO, as determined by Argyle, *et al.*¹⁵ If we assume that the variation of the edge is due to a shift of the conduction band, we can account for the depopulation of the conduction band with increasing temperature by a transfer of carriers to a trap level whose energy is relatively independent of temperature and magnetic field and which crosses the bottom of the conduction band at 50°K. A similar model has been proposed for CdCr_2Se_4 by Lehmann.¹⁶

Section I

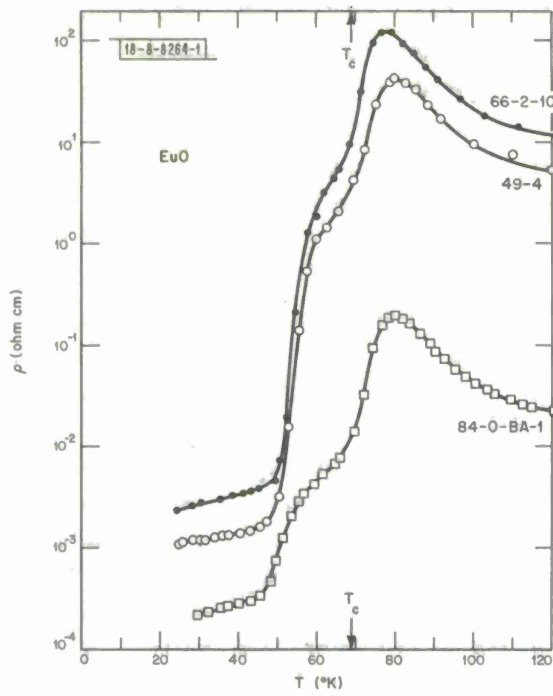


Fig. I-9. Resistivity vs temperature of three moderately conducting EuO samples.

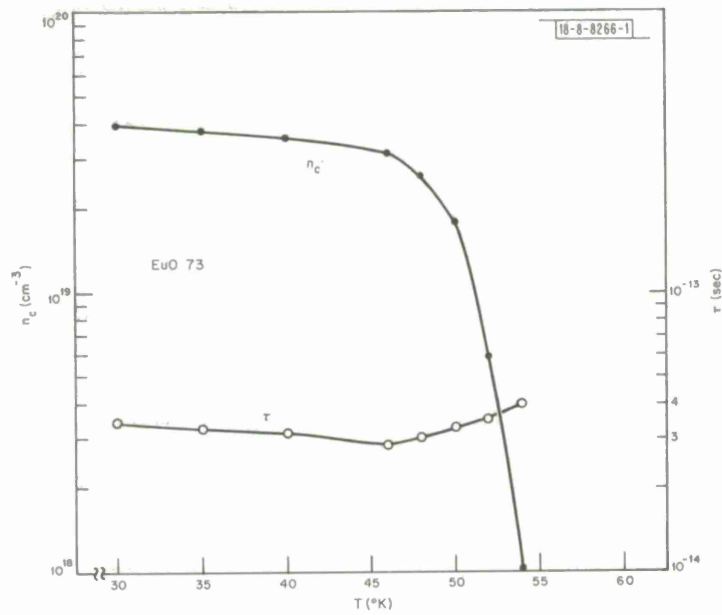


Fig. I-10. Carrier concentration and scattering time of EuO sample, computed from optical absorption and conductivity measurements.

With these restrictions, the model can be made to agree quantitatively with the data obtained on a large variety of samples. In each case, agreement is obtained assuming that the trap level - band edge crossing occurs at about 50°K and, in the moderate conductivity range ($10^{-1} \text{ ohm-m} < \rho_{\text{max}} < 10^5 \text{ ohm-cm}$), that the trap level density is approximately equal to the electron density. Figure I-11 shows the resistivity vs temperature for an EuO sample at $H = 0$ and 48 kG. A theoretical curve based on the model is also shown for $H = 0$. The fit was obtained assuming the number of traps is equal to the number of conduction electrons. The deviation between theory and experiment in the range between 75° and 80°K could be due to variations in mobility not accounted for in the model.

For slightly fewer electrons than traps, the Fermi level of the system remains tied to the trap level and the population of the conduction band is governed primarily by a Boltzmann factor $\exp(-\Delta E/kT)$, where ΔE is the energy separation between the trap level and the bottom of the conduction band. For this case, the resistivity curve will have a relatively broad peak near the temperature where $(d/dT)(\Delta E/kT) = 0$. Small variations in the ratio of electron density to trap state density about the value unity result in large variations in total resistivity change and can totally account for the variation between samples. Although the identity of the trap state has not been determined by these measurements, its apparent lack of dependence on temperature or magnetic field may indicate that it is nonmagnetic in character.

This model also accounts for the negative magnetoresistance of EuO. As Argyle and Miyata¹⁷ have demonstrated, an applied magnetic field decreases the magnetic energy in the vicinity of the Curie point. In our model, this will lower the band edge and two effects will occur: (a) the elbow will move to a higher temperature, and (b) the ρ vs T slope will be more gradual. As seen in Fig. I-11, the shift in the elbow is about 10°K for the 48-kG field. The calculated shift for an 18-kG field, the highest studied by Argyle and Miyata, is about 3°K . Our 48-kG results are consistent with a reasonable extrapolation from their data.

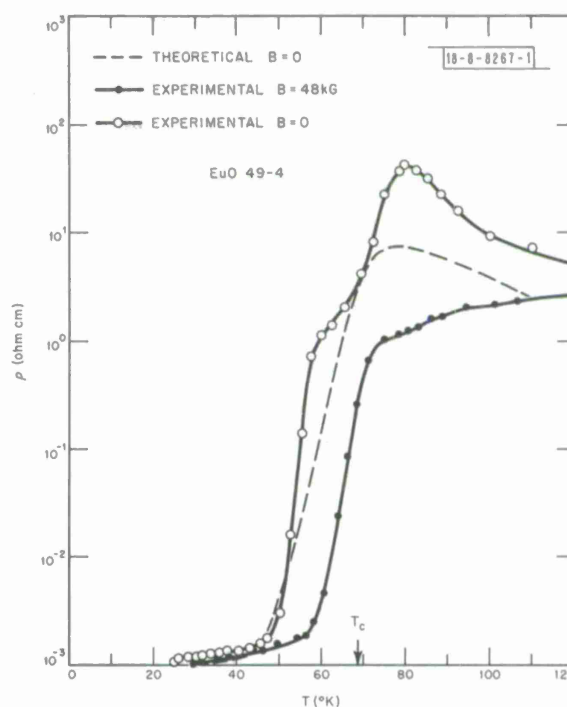


Fig. I-11. Resistivity vs temperature of EuO sample with $H = 0$ and 48 kG. Theoretical curve (see text) is also shown for $H = 0$.

M. R. Oliver
J. O. Dimmock
T. B. Reed

REFERENCES

1. G. E. Stillman, C. M. Wolfe, and J. O. Dimmock, *Solid State Commun.* 7, 921 (1969), DDC AD-693903.
2. G. E. Stillman, C. M. Wolfe, I. Melngailis, C. D. Parker, P. E. Tannenwald, and J. O. Dimmock, *Appl. Phys. Letters* 13, 83 (1968), DDC AD-681589.
3. D. J. Oliver, *Phys. Rev.* 127, 1045 (1962); R. A. Reynolds, *Solid-State Electron.* 11, 385 (1968).
4. I. Melngailis and A. G. Milnes, *J. Appl. Phys.* 33, 995 (1962).
5. M. A. C. S. Brown, and M. F. Kimmitt, *Brit. Commun. and Electron.* 10, 608 (1963); J. R. Apel, T. O. Poehler, and C. R. Westgate, *Appl. Phys. Letters* 14, 161 (1969).
6. E. Burstein, G. Picus, and N. Sclar, *Proceedings of the Photoconductivity Conference, Atlantic City, 1954* (Wiley, New York, 1956), p. 353.
7. R. Solomon, *Proceedings of the International Symposium on GaAs, Dallas, 1968* (Institute of Physics and The Physical Society, London, 1969), p. 17.
8. B. F. Lewis and E. H. Sondheimer, *Proc. Roy. Soc. (London)* A227, 241 (1954).
9. S. S. Devlin, in *Physics and Chemistry of II-VI Compounds*, edited by M. Aven and J. S. Prener (North-Holland Publishing Co., Amsterdam, 1967), p. 551; S. S. Devlin, Thesis, Case Institute of Technology (1964).
10. S. J. Fray, F. A. Johnson, J. E. Quarrington, and N. Williams, *Proc. Phys. Soc. (London)* 77, 215 (1961).
11. C. E. Hurwitz, M. R. Oliver, J. O. Dimmock, and T. B. Reed, *Bull. Am. Phys. Soc. II* 14, 309 (1969).
12. T. Kasuya and A. Yanase, *Rev. Mod. Phys.* 40, 684 (1968).
13. M. J. Freiser, F. Holtzberg, S. Methfessel, G. D. Pettit, M. W. Shafer, and J. C. Suits, *Helv. Phys. Acta* 41, 832 (1968).
14. G. Busch and P. Wachter, *Z. angew. Phys.* 26, 1 (1968).
15. B. E. Argyle, N. Miyata, and T. D. Schultz, *Phys. Rev.* 160, 413 (1967).
16. H. W. Lehmann, *Phys. Rev.* 163, 488 (1967).
17. B. E. Argyle and N. Miyata, *Phys. Rev.* 171, 555 (1968).

II. MATERIALS RESEARCH

A. CALCULATION OF THE LIQUIDUS-SOLIDUS GAP IN HOMOGENEOUS, MONOTONIC ALLOY SYSTEMS

The general expression for the thermodynamic relationship between liquidus and solidus equilibrium compositions [Ref. 1, Eq. (II-3)] has been applied to alloy systems which exhibit complete miscibility in the liquid and solid phases and are characterized by monotonic variations in liquidus and solidus temperatures with composition. By considering the free-energy curves for such homogeneous and monotonic systems, it can be shown that the excess molar free energies of mixing for the two phases, and their difference, are small. The nonideal term D in the general equation, which is equal to the difference between the partial excess free energies of mixing, can therefore be neglected, in which case the general equation is replaced by the simple form of the ideal equation [Ref. 1, Eq. (II-6)]. As indicated previously,¹ the ideal equation is of particular interest because it makes it possible, without using theoretical solution models or adjustable parameters, to calculate one of the boundaries of the two-phase field when the other boundary and the enthalpies of fusion of the pure components are known.

The ideal equation has been used to calculate solidus curves for a large number of binary and pseudobinary systems from experimental liquidus and enthalpy data. For many of these systems (InAs-GaAs, InSb-InAs, InSb-GaSb, GaSb-AlSb, CdTe-ZnTe, CdTe-CdSe, and HgTe-CdTe), the calculated curves are in good to excellent agreement with published experimental solidus values. For three systems (Ag-Au, SnTe-PbTe, and InAs-InP), they show excellent agreement with the results of the most recent investigations. For the Cu-Ni, Ge-Si, and HgTe-HgSe systems, however, discrepancies between the calculated curves and experimental data (Figs. II-1 through II-3) indicate the need for a critical re-evaluation of the presently available solidus data. As suggested by several authors, it is likely that the experimental data for these systems were not obtained under essentially equilibrium conditions.

J. Steininger

B. SOLIDUS CURVE AND CRYSTAL GROWTH OF CdTe-ZnTe ALLOYS

Our earlier study of liquid-solid phase equilibria in the Zn-Cd-Te ternary system² has been extended by determining the pseudobinary CdTe-ZnTe solidus curve.

Solidus arrest temperatures were found by thermal analysis of heating curves. The alloy samples were prepared in evacuated and sealed fused silica ampoules by solidification from the melt and then annealed for at least 16 hours at 20°C below the estimated solidus temperature. X-ray powder analysis of samples annealed in this way showed no evidence of inhomogeneity, and gave lattice parameters in agreement with published values. The temperature of each thermal arrest was obtained from the intersection of the nearly straight lines below and above the solidus break on a temperature-vs-time plot. More prolonged annealing resulted in sharper breaks but did not cause any substantial displacement of the intersections. The reproducibility of the arrests was about $\pm 3^\circ\text{C}$.

Section II

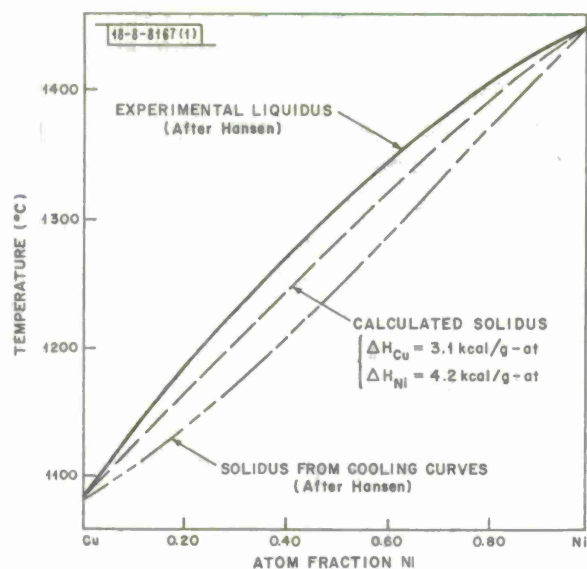


Fig. II-1. Phase diagram of Cu-Ni system. Experimental curves after M. Hansen, *Constitution of Binary Alloys* (McGraw-Hill, New York, 1958), p. 602.

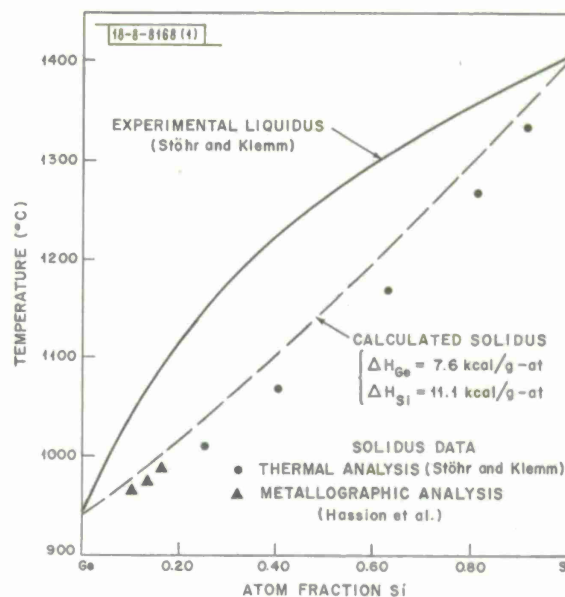


Fig. II-2. Phase diagram of Ge-Si system. Experimental curves after H. Stöhr and W. Klemm, *Z. anorg. allg. Chem.* **241**, 305 (1939) and F. X. Hasson, *et al.*, *J. Phys. Chem.* **59**, 1118 (1955).

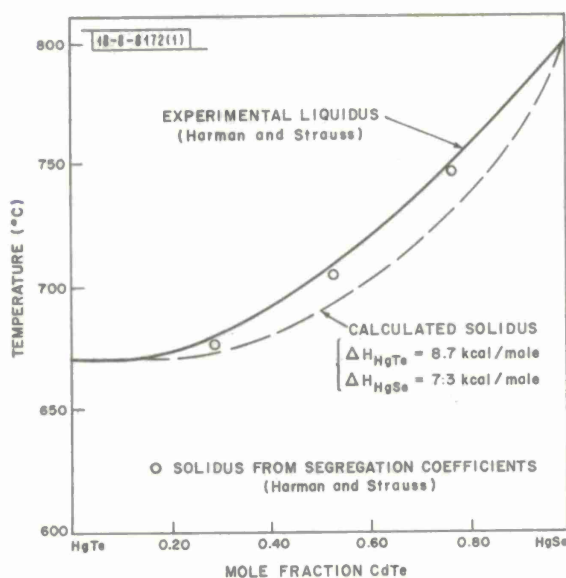


Fig. II-3. Phase diagram of HgTe-HgSe system. Experimental data after Harman and Strauss, Ref. 3.

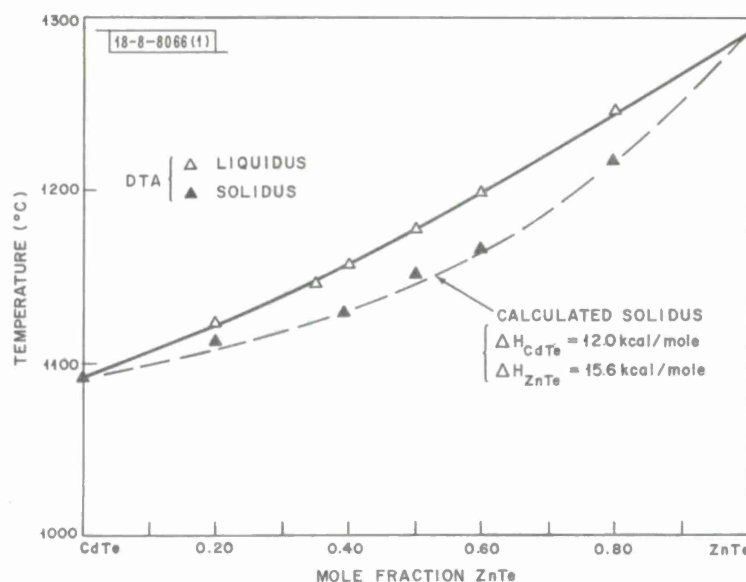


Fig. II-4. Phase diagram of CdTe-ZnTe system.

The CdTe-ZnTe solidus arrests are plotted against composition in Fig. II-4, together with data reported earlier² for the liquidus arrests. Both liquidus and solidus temperatures increase monotonically and sublinearly with increasing ZnTe concentration. This type of variation, which indicates small positive deviations from ideality, slightly larger in the solid phase, has also been reported for other pseudobinary II-VI systems such as HgTe-HgSe (Ref. 3), ZnTe-ZnSe (Ref. 4) and CdTe-CdSe (Ref. 5).

The dashed line in Fig. II-4 represents the solidus curve calculated from the ideal liquidus-solidus equation [Ref. 1, Eq. (II-6)] using experimental liquidus² and enthalpy of fusion⁶ data. The agreement between calculated and experimental values is excellent ($\pm 3^\circ\text{C}$) over the entire composition range, thereby confirming that the deviations from ideality in the two phases are small and nearly equal.¹

Because of the relatively narrow liquidus-solidus gap in this system, it has been possible to grow homogeneous alloy crystals by using the Bridgman method for directional freezing of stoichiometric melts in sealed fused silica ampoules. To minimize homogenization of the melt, ampoules about 1 cm in diameter and freezing rates of about 2 cm/day were used. The results of electron microprobe analysis of an alloy ingot grown by this technique are plotted in Fig. II-5. The ingot has a typical diffusion-controlled profile,⁷ with an initial transient of slowly increasing CdTe concentration, a steady-state region with composition equal to the initial melt composition of 50 mole percent CdTe, and a final transient of rapidly increasing CdTe concentration. Crystals from the middle section of this ingot were homogeneous and showed no evidence of dendritic or cellular growth.

The composition of the first-to-freeze section of the ingot is 35 mole percent CdTe, in excellent agreement with the phase diagram obtained by thermal analysis. The amount of solute accumulated in the boundary layer was determined by integration of the concentration along

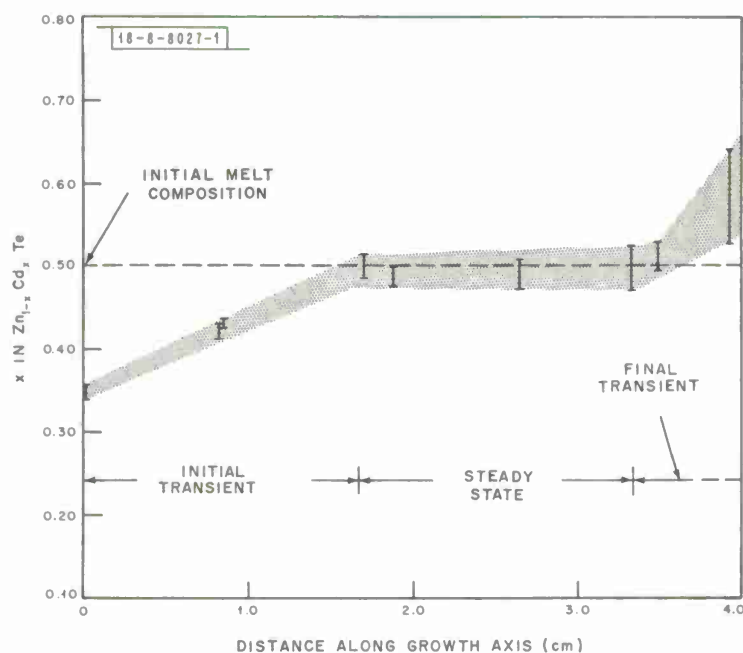


Fig. II-5. Composition profile of CdTe-ZnTe alloy ingot.

the initial transient and used to calculate the diffusion coefficient in the steady-state region.⁷ A value of $5.6 \times 10^{-5} \text{ cm}^2/\text{sec}$ was obtained. The minimum temperature gradient required to avoid constitutional supercooling was then calculated to be $35^\circ\text{C}/\text{cm}$, in good agreement with the experimental evidence.

J. Steininger
M. C. Finn
R. E. England

C. PREPARATION OF TELLURATES BASED ON NaSbO_3 AND LiSbO_3

The preparation of an extended series of tellurates based on the PbSb_2O_6 structure⁸ suggested the possibility of preparing analogous compounds based on the alkali antimonates NaSbO_3 and LiSbO_3 . A large number of such tellurates have now been prepared by sintering stoichiometric mixtures of oxides and carbonates. Three different types of crystal structure are observed: the NaSbO_3 ilmenite structure (an ordered corundum structure in which the hexagonal close-packed oxygen lattice is interleaved with layers of Na and Sb which are two-thirds occupied), the LiSbO_3 structure, and a hexagonal structure which has not been identified.

The compounds prepared with the ilmenite structure are $\text{Na}_2\text{TiTeO}_6$, $\text{Na}_2\text{GeTeO}_6$, $\text{Li}_2\text{GeTeO}_6$, $\text{Li}_2\text{Mn}_{0.1}\text{Ge}_{0.9}\text{TeO}_6$, LiCdCrTeO_6 , LiCdGaTeO_6 , and LiAlMgTeO_6 . Their lattice parameters, sintering temperatures and times, and colors are listed in Table II-1. The latter three compounds are of interest because Cr_2O_3 , Ga_2O_3 , and Al_2O_3 crystallize in the corundum structure but with much smaller lattice constants ($a = 4.952$, 4.979 , and 4.763 \AA , respectively; $c = 13.584$, 13.429 , 13.003 \AA , respectively), and the bonding should be quite different since the $(\text{TeO}_6)^{6-}$ group forms a strong complex.

TABLE II-1
PROPERTIES OF TELLURATES BASED ON NaSbO_3 AND LiSbO_3

Ilmenite Structure					
	Lattice Parameters (Å)		Sintering Temperature (°C)	Sintering Time (hours)	Color
	a	c			
$\text{Na}_2\text{TiTeO}_6$	5.215	15.818	720	3	Light yellow
$\text{Na}_2\text{GeTeO}_6$ (low temperature)	5.096	15.958	650	10	White
$\text{Li}_2\text{GeTeO}_6$	5.003	14.318	750	1	White
$\text{Li}_2\text{Mn}_{0.1}\text{Ge}_{0.9}\text{TeO}_6$	5.004	14.323	700	1	Orange
LiCdCrTeO_6	5.167	14.740	650	3	Green
LiCdGaTeO_6	5.159	14.788	700	5	White
LiAlMgTeO_6	4.989	14.003	700	2	White
$\text{Na}_2\text{MnTeO}_6$ Structure					
$\text{Na}_2\text{MnTeO}_6$	5.109	10.556	700	1	Brown red
$\text{Na}_2\text{SnTeO}_6$	5.337	10.684	810	3	White
$\text{Na}_2\text{GeTeO}_6$ (high temperature)	5.095	10.631	760	1	White

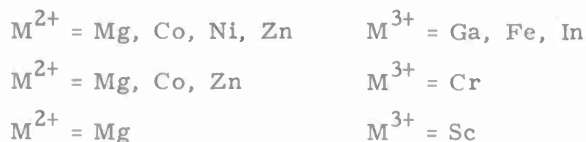
The compounds $\text{Na}_2\text{MnTeO}_6$ and $\text{Na}_2\text{SnTeO}_6$ have a hexagonal structure which has not been identified. Their lattice parameters, sintering temperatures and times, and colors are also listed in Table II-1. The same structure is obtained when $\text{Na}_2\text{GeTeO}_6$, which has the ilmenite structure at room temperature, is heated to 750°C. Comparison of the lattice parameters of the two forms of $\text{Na}_2\text{GeTeO}_6$ shows that the a parameters are the same while the c parameter of the high-temperature modification is about two-thirds that of the low-temperature form. This indicates that the two forms have the same oxygen packing and array in layers of $2\text{Na}^+ - \text{Ge}^{4+} \text{Te}^{6+} - 2\text{Na}^+$, but differ in the arrangement of the cation layers with respect to each other.

Whether the ilmenite or $\text{Na}_2\text{MnTeO}_6$ structure will be formed is not determined solely by the size of the 4+ ion, since the former structure is obtained for $\text{Na}_2\text{TiTeO}_6$ and the latter for both $\text{Na}_2\text{MnTeO}_6$ and $\text{Na}_2\text{SnTeO}_6$, although the Ti^{4+} ion is intermediate in size between Mn^{4+} and Sn^{4+} (see lattice parameters in Table II-1). It is concluded that the stability of Ti^{4+} in distorted octahedral coordination causes $\text{Na}_2\text{TiTeO}_6$ to have the ilmenite structure with face-shared Na^+ and Ti^{4+}

Section II

octahedra, and that in the $\text{Na}_2\text{MnTeO}_6$ structure the oxygen octahedra of Mn^{4+} , Sn^{4+} , or Ge^{4+} share only edges with those of Na^+ .

The tellurates found to have the LiSbO_3 structure are $\text{Li}_2\text{MnTeO}_6$, $\text{Li}_2\text{SnTeO}_6$, and $\text{Li}_2\text{TiTeO}_6$, as well as a number of compounds which have the formula $\text{LiM}^{2+}\text{M}^{3+}\text{TeO}_6$ with



The compounds LiNiCrTeO_6 , LiCdFeTeO_6 , LiCdRhTeO_6 , LiCdInTeO_6 , and LiCaInTeO_6 have x-ray powder patterns containing not only the lines of the LiSbO_3 structure but also some characteristic additional lines which indicate a superstructure or low symmetry distortion for these compounds.

H. M. Kasper

D. PREPARATION AND MAGNETIC PROPERTIES OF RUTHENIUM SPINELS

Investigations of 2,5- and 2,6-spinels have shown that it is possible to prepare compounds like $\text{Co}_7\text{Sb}_2\text{O}_{12}$ and Co_5TeO_8 which have Co^{2+} , Ni^{2+} , or Zn^{2+} in octahedral sites and Co^{2+} or Zn^{2+} in tetrahedral sites. There are a number of 2,4-spinels where the octahedral sites are occupied by Ti^{4+} , V^{4+} , Mn^{4+} , Sn^{4+} , and Pt^{4+} , but no spinel of Ru^{4+} has been reported. To prepare such a compound, Co_2RuO_4 , stoichiometric amounts of CoCO_3 (reagent grade) and Ru metal (99.9 percent) were mixed and slowly heated in air to 900°C , then reground and pressed to a disk, which was reacted in air at 1200°C . The resulting material was ground in an agate mortar and investigated by x-ray diffraction. The powder pattern showed the characteristic lines of a spinel phase with a lattice constant of 8.306\AA . The spinel ZnCoRuO_4 with a lattice constant of 8.358\AA has been prepared in a similar way. It is expected that the octahedral sites are occupied by Ru^{4+} and Co^{2+} , since there is no known compound in which Ru^{4+} occupies tetrahedral sites. The lattice constants are smaller than in other spinels with Co^{2+} on octahedral sites (Co_5TeO_8 , 8.546\AA ; $\text{Co}_7\text{Sb}_2\text{O}_{12}$, 8.523\AA ; and Co_2TiO_4 , 8.465\AA) and indicate a considerable interaction of O^{2-} with the Co^{2+} and Ru^{4+} in the octahedral sites.

The magnetic susceptibility of Co_2RuO_4 between 4.2° and 300°K exhibits approximately Curie-Weiss behavior with $\Theta_a = 20^\circ\text{K}$. The Néel temperature is approximately 20°K . The effective magnetic moment is $\mu_{\text{eff}} = 4.1\mu_B$. It is assumed that this is mainly due to Co^{2+} in tetrahedral sites and that the strong interaction of O^{2-} with Co^{2+} and Ru^{4+} in the octahedral sites considerably reduces the observed moment at temperatures below 300°K .

H. M. Kasper

E. STRUCTURE AND MAGNETIC PROPERTIES OF VOSO_4

Anhydrous VOSO_4 exists in two modifications at room temperature: α - VOSO_4 is tetragonal⁹ and is formed by dehydration of its hydrates below 280°C ; β - VOSO_4 is orthorhombic and may be prepared either from the reaction of H_2SO_4 and V_2O_5 (Ref. 10) or by dehydration above 280°C . The orthorhombic structure has chains of corner-shared VO_6 octahedra connected by corner-shared SO_4 tetrahedra to form a three-dimensional network.¹¹ As an extension of structural

studies on orthorhombic β -VOSO₄ (Ref. 11) and tetragonal NbOPO₄ (Ref. 12), the structure of tetragonal α -VOSO₄ has been investigated.

Preliminary analysis of the x-ray powder data presented by Tudo⁹ indicated that the structure of α -VOSO₄ was probably that of NbOPO₄ (Ref. 12), MoOPO₄ (Ref. 13), and VOMoO₄ (Ref. 14). Since α -VOSO₄ is obtained only by dehydration, single crystals are not available, and confirmation of the proposed structure has been obtained by quantitative treatment of x-ray powder diffraction data. Independently, Ladwig¹⁵ has proposed the same structure for α -VOSO₄ based on qualitative interpretation of x-ray powder diagrams, electron diffraction patterns, and IR spectra.

The α -VOSO₄ studied was prepared by the dehydration of a commercially available hydrate (Fisher purified) in three steps. After this hydrate was heated in air for many hours in a 130°C drying oven to obtain the monohydrate, the sample was transferred to a tube furnace and heated to 260°C in a stream of dry nitrogen for 4 hours. Finally, the sample, still under flowing nitrogen, was heated to 350°C for 1/2 hour to improve its crystallinity, thus making it less susceptible to rehydration and improving its x-ray pattern. Before this last step, all lines of the x-ray pattern except those of the hk0 and h00 type were somewhat broadened. However, it was found that heating the α -form for long periods of time above 260°C gradually converted it to the orthorhombic β -form.

A Norelco vertical diffractometer with monochromated (LiF crystal) CuK α radiation was used to collect the x-ray intensity data at room temperature. To prevent rehydration of the sample, the entire diffractometer was covered with a plastic bag and flooded with dry nitrogen. Crystallographic studies at high temperature were made using a Tem-Pres furnace attachment and a General Electric diffractometer with the sample maintained in a continuous flow of dry nitrogen. The intensity data were collected either by measuring the area under the peaks on a slow-scanned (1/4°/min.) diffraction pattern or by accumulating counts while slow scanning through a peak. Where reflections overlapped, they were measured as a single intensity. The data were computer analyzed by the simplex method to refine atomic positional parameters and cell temperature factor. The same method was used to refine cell dimensions.

At room temperature, the tetragonal cell dimensions of our sample of α -VOSO₄ are found to be $a = 6.261 \pm 0.003 \text{ \AA}$, $c = 4.101 \pm 0.003 \text{ \AA}$, and $c/a = 0.655$. These are to be compared to Tudo's⁹ values of $a = 6.267 \text{ \AA}$, $c = 4.119 \text{ \AA}$, and $c/a = 0.657$. Tudo's larger c-axis suggests that his sample retained a trace of water.

Our most reliable set of data, containing nineteen observed intensities, shows good agreement with the proposed MoOPO₄ structure type having the atomic positions listed in Table II-2. Refinement of the atomic parameters based on minimization of a discrepancy factor $R = \sum |I_o - I_c| / \sum I_o$ indicated that the strongest reflection (200) had too much influence on the structure determination. Refinement of the data with this reflection removed resulted in a much better overall fit of intensities and an R factor of 0.094. The final atomic parameters and cell temperature factor are also listed in Table II-2. A comparison of observed and calculated intensities is given in Table II-3. Near-neighbor interatomic distances and selected bond angles calculated from the above parameters are listed in Table II-4. They are all consistent with the known structural chemistry of the vanadyl and sulfate ions.

TABLE II-2
CRYSTAL STRUCTURE OF α -VOSO₄

Space Group	P4/n (No. 85)
Unit Cell Dimensions	$a = 6.261 \pm 0.003 \text{ \AA}$ $c = 4.101 \pm 0.003 \text{ \AA}$
Cell Contents: 2 VOSO ₄	
V in 2(c)	0, 1/2, z; 1/2, 0, \bar{z} ($z = 0.6176 \pm 0.0010$)
O _I in 2(c)	0, 1/2, z; 1/2, 0, \bar{z} ($z = 0.220 \pm 0.004$)
S in 2(b)	0, 0, 1/2; 1/2, 1/2, 1/2
O _{II} in 8(g)	$x, y, z; \bar{x}, \bar{y}, z; 1/2 + x, 1/2 + y, \bar{z}; 1/2 - x, 1/2 - y, \bar{z};$ $\bar{y}, x, \bar{z}; y, \bar{x}, \bar{z}; 1/2 - y, 1/2 + x, z; 1/2 + y, 1/2 - x, z$ $x = 0.538 \pm 0.003, y = 0.683 \pm 0.003, z = 0.285 \pm 0.003$
Cell Temperature Factor	B = 0.4

TABLE II-3
OBSERVED AND CALCULATED INTENSITIES FOR α -VOSO₄

I_{obs}	I_{calc}	hkl	d_{calc}	I_{obs}	I_{calc}	hkl	d_{calc}
2	1	110	4.427	1	1	202	1.715
51	51	001	4.101	5	$\begin{Bmatrix} 5 \\ 3 \end{Bmatrix}$	$\begin{Bmatrix} 212 \\ 122 \end{Bmatrix}$	1.654
20	20	101	3.431	2	$\begin{Bmatrix} 3 \\ 1 \end{Bmatrix}$	$\begin{Bmatrix} 321 \\ 231 \end{Bmatrix}$	1.599
100 [†]	$\begin{Bmatrix} 87 \\ 2 \end{Bmatrix}$	$\begin{Bmatrix} 200 \\ 111 \end{Bmatrix}$	$\begin{Bmatrix} 3.130 \\ 3.009 \end{Bmatrix}$	16	11	400	1.565
35	35	201	2.488	5	5	222	1.504
6	$\begin{Bmatrix} 10 \\ 0.1 \end{Bmatrix}$	$\begin{Bmatrix} 211 \\ 121 \end{Bmatrix}$	2.312	19	$\begin{Bmatrix} 3 \\ 8 \\ 7 \end{Bmatrix}$	$\begin{Bmatrix} 330 \\ 302 \\ 401 \end{Bmatrix}$	$\begin{Bmatrix} 1.476 \\ 1.463 \\ 1.462 \end{Bmatrix}$
10	9	220	2.214	8	$\begin{Bmatrix} 7 \\ 2 \\ 1 \\ 0.1 \end{Bmatrix}$	$\begin{Bmatrix} 312 \\ 132 \\ 411 \\ 141 \end{Bmatrix}$	$\begin{Bmatrix} 1.424 \\ 1.424 \end{Bmatrix}$
3	2	002	2.050	10	$\begin{Bmatrix} 2 \\ 8 \end{Bmatrix}$	$\begin{Bmatrix} 420 \\ 240 \end{Bmatrix}$	1.400
15	$\begin{Bmatrix} 10 \\ 2 \end{Bmatrix}$	$\begin{Bmatrix} 310 \\ 130 \end{Bmatrix}$	1.980				
26	$\begin{Bmatrix} 14 \\ 12 \end{Bmatrix}$	$\begin{Bmatrix} 102 \\ 221 \end{Bmatrix}$	$\begin{Bmatrix} 1.949 \\ 1.948 \end{Bmatrix}$				
16	$\begin{Bmatrix} 15 \\ 1 \end{Bmatrix}$	$\begin{Bmatrix} 112 \\ 301 \end{Bmatrix}$	$\begin{Bmatrix} 1.861 \\ 1.860 \end{Bmatrix}$				
0	$\begin{Bmatrix} 0.2 \\ 0.1 \end{Bmatrix}$	$\begin{Bmatrix} 131 \\ 311 \end{Bmatrix}$	1.783				
† Not used in refinement.							

TABLE II-4
SOME INTERATOMIC DISTANCES (Å) AND ANGLES IN α -VOSO₄

V-O (± 0.03)	O-O (± 0.04)
V - 2O _I (O _I - 2V) = 1.63, 2.47	O _I - 4O _{II} = 2.85 [†]
V - 4O _{II} (O _{II} - V) = 2.04	4O _{II} = 2.88 [†]
O _I - V - O _{II} = 101°, 79°	4O _{II} = 3.12
O _{II} - V - O _{II} = 88°	(O _{II} - 3O _I) = (2.85, 2.88, 3.12)
	O _{II} - 2O _{II} = 2.83 [†]
	2O _{II} = 2.42 [‡]
S-O (± 0.02)	2O _{II} = 2.86
S - 4O _{II} (O _{II} - S) = 1.46	O _{II} = 2.34 [‡]
O _{II} - S - O _{II} = 111°, 106°	O _{II} = 3.29
	O _{II} = 3.63
[†] Interatomic distances within VO ₆ octahedra. [‡] Interatomic distances within SO ₄ tetrahedra.	

The crystal structure of α -VOSO₄ may be described as continuous chains of corner-shared VO₆ octahedra running parallel to the *c*-axis. Each chain is connected to four other chains by corner sharing with sulfate tetrahedra, as shown in Fig. II-6. Alternatively, the structure may be described as a distortion of a cubic-close-packed oxygen lattice in which one-fifth of the octahedral sites are occupied by vanadium and one-tenth of the tetrahedral sites are occupied by sulfur.¹⁴ An undistorted cubic-close-packed arrangement of this type would have a *c/a* ratio of 0.632 and an oxygen volume of 15.5 Å³ (*r* = 1.40 Å). In α -VOSO₄, we find *c/a* = 0.655 and an oxygen volume of 16.08 Å³, indicating that the distortion of the oxygen lattice from a close-packed arrangement is small.

Although the oxygens surrounding a vanadium ion form almost perfect octahedra, the vanadium ions are cooperatively displaced from the centers of the octahedra to form one very short (1.63 Å) vanadium-oxygen bond characteristic of the vanadyl ion, as illustrated in Fig. II-7. This short vanadyl bond is also present in similar compounds such as VOMoO₄ (1.677 Å, Ref. 14), β -VOSO₄ (1.594 Å, Ref. 11) and VOSO₄ · 5H₂O (1.591 Å, Ref. 16). Vanadium is bonded to four other oxygens at 2.04 Å giving it a fivefold coordination. The last oxygen of the octahedra is 2.47 Å from the vanadium and must be only weakly bonded. This very large V-O_I distance has the effect of breaking the chains of octahedra and gives the structure a layered character. This is supported by our observation that all lines, except the *hk*0 type, gradually broadened and weakened on absorption of water. Ladwig¹⁵ has discussed the mechanism of hydration to VOSO₄ · H₂O in terms of this layer structure.

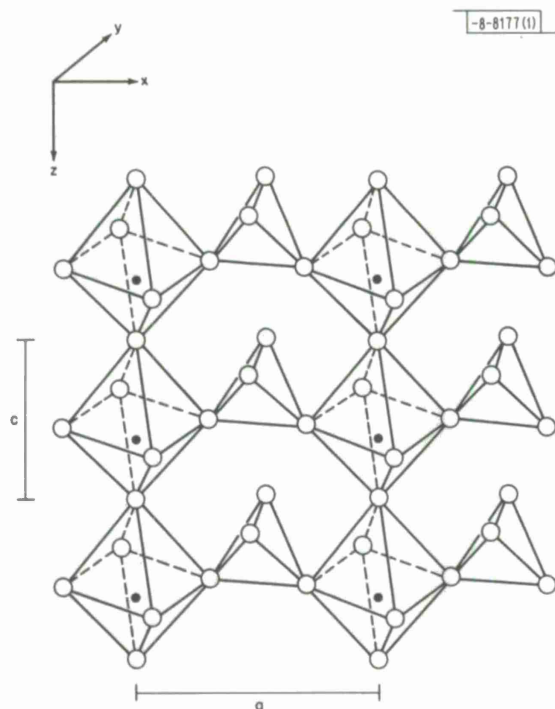


Fig. II-6. 001 view of α -VOSO₄, showing chains of VO₆ octahedra cross-linked by SO₄ tetrahedra.

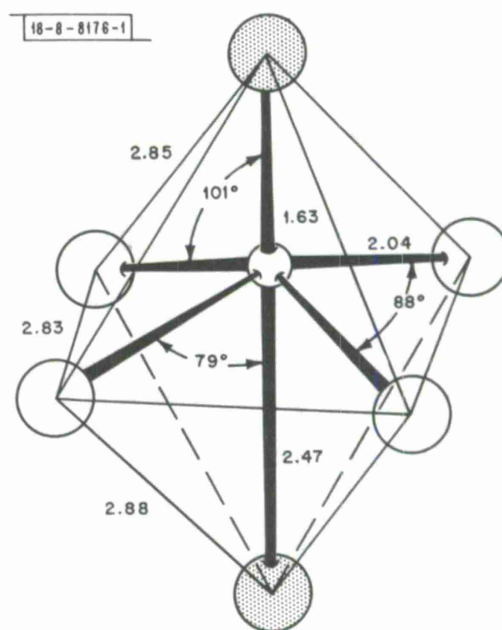


Fig. II-7. Oxygen coordination with vanadium (small circle) in α -VOSO₄. O₁ is shaded.

Section II

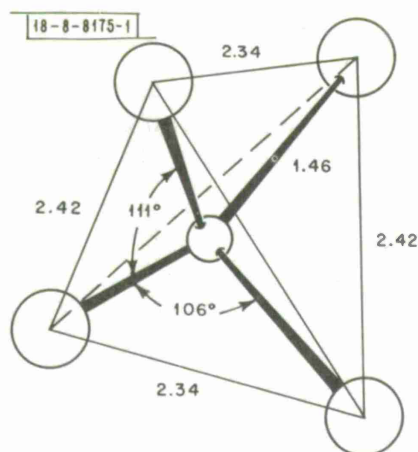


Fig. II-8. Oxygen coordination with sulfur (small circle) in α - VOSO_4 .

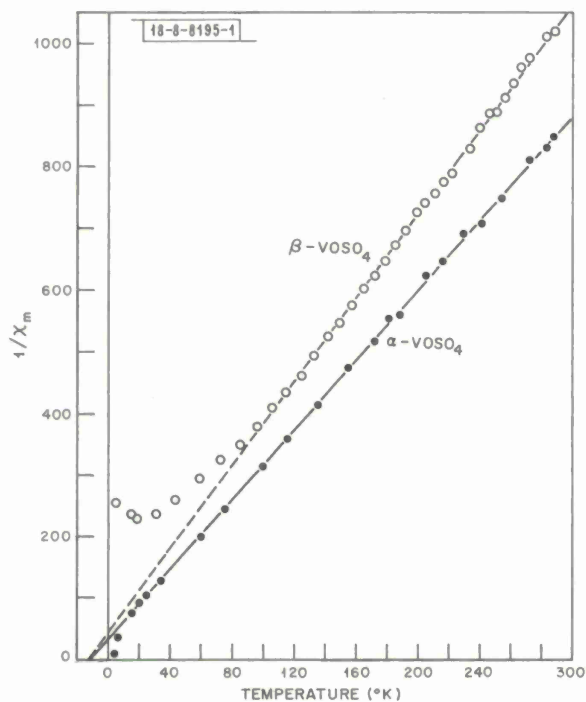


Fig. II-9. Reciprocal molar magnetic susceptibility vs temperature for α - VOSO_4 and β - VOSO_4 .

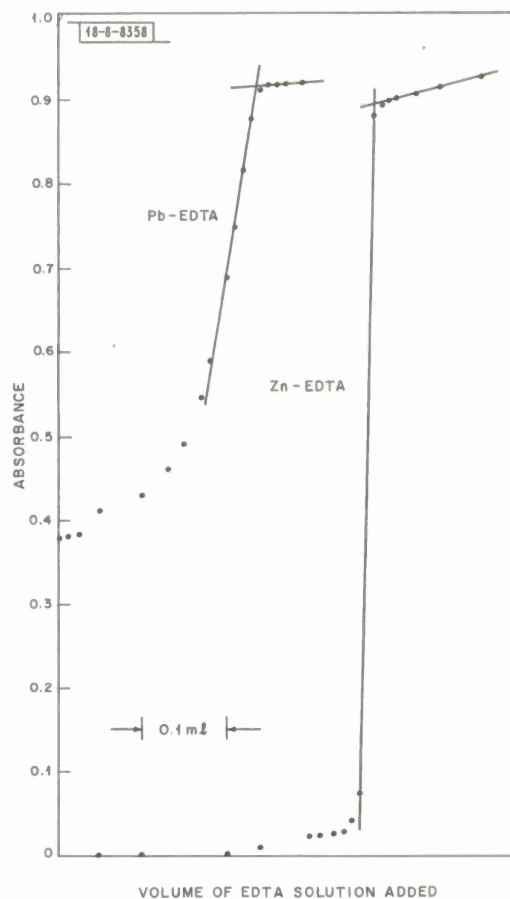


Fig. II-10. Absorbance vs volume of EDTA solution added for photometric EDTA titrations of Zn and Pb.

The SO_4 tetrahedra are only slightly elongated along the c-axis, as shown in Fig. II-8. The sulfur-oxygen distance of 1.46 \AA in $\alpha\text{-VOSO}_4$ is very similar to the average S-O distance of 1.430 \AA found in $\beta\text{-VOSO}_4$ (Ref. 11) and is within the range 1.44 to 1.53 \AA given in the International Tables.¹⁷

X-ray diffraction measurements on $\alpha\text{-VOSO}_4$ up to 400°C showed that in this temperature range this phase converts only slowly to the β -phase. The cell dimensions increase smoothly with temperature and at 400°C are $a = 6.283 \pm 0.010$, $c = 4.185 \pm 0.010$, and $c/a = 0.666$. The thermal expansion coefficients based on the data, $\alpha_a = 8 \times 10^{-6} \text{ deg}^{-1}$ and $\alpha_c = 50 \times 10^{-6} \text{ deg}^{-1}$, show that the distances in the c-direction increase with temperature about six times as fast as the distances in the a-direction, strongly reflecting the layered nature of this structure. Intensity data collected at 400°C , while not as reliable as the room-temperature data, gave essentially the same structure, the increase in the c-axis being largely confined to an increase in the long V-O₁ distance.

All magnetic measurements were made with a vibrating-sample magnetometer calibrated with nickel metal. Both the α - and β -forms were studied from 4.2°K to room temperature and in magnetic fields to 17.2 kOe . Samples of about 100 mg were placed in teflon containers which, in the case of the hygroscopic α -form, were sealed with paraffin.

The two structural forms of anhydrous VOSO_4 exhibit very different magnetic properties. Above 10°K , the α -form obeys the Curie-Weiss law $\chi_m = C_m/(T - \Theta)$ with $C_m = 0.355$ ($\mu_{\text{eff}} = 1.69 \mu_B$) and $\Theta = -12^\circ\text{K}$ (Fig. II-9). The theoretical spin-only value of μ_{eff} for V^{4+} ($3d^1$) is $1.73 \mu_B$. Recently, Edge¹⁸ has reported that at room temperature the susceptibility of $\alpha\text{-VOSO}_4$ "corresponded to one unpaired electron per vanadium." Doyle, *et al.*¹⁹ have reported an effective magnetic moment of $1.34 \mu_B$ for VOMoO_4 based on a single measurement at 20°C and the assumption $\Theta = 0^\circ\text{K}$. Their low μ_{eff} is compatible with a $\Theta < 0^\circ\text{K}$.

Below 10°K , the susceptibility of $\alpha\text{-VOSO}_4$ increases sharply and continuously to 4.2°K where it reaches about $\frac{1}{3} \mu_B/\text{V}^{4+}$. Field studies to 17.2 kOe at 4.2°K showed the nonlinear effects of saturation that are characteristic of ferro- or ferrimagnetism while the magnetization at 77°K and room temperature increases linearly with field, characteristic of paramagnetism. Such a large moment per V^{4+} ion is difficult to attribute to impurities since x-ray patterns of samples studied never showed detectable second phases. The negative value for Θ points to a ferrimagnetic order of vanadium, and inspection of the structure indicates that the order is probably complex. A Curie temperature close to 4.2°K is indicated, since the magnetization is still increasing sharply with decreasing temperature.

For $\beta\text{-VOSO}_4$ prepared from solution, the susceptibility obeys the Curie-Weiss law above 100°K with $C_m = 0.296$ ($\mu_{\text{eff}} = 1.54 \mu_B$) and $\Theta = -12^\circ\text{K}$ (Fig. II-9). The effective moment per V^{4+} ion in its paramagnetic temperature region is lower than the theoretical spin-only value or the experimental value found in $\alpha\text{-VOSO}_4$. Both forms of VOSO_4 have the same value for Θ , indicating that the predominant V-SO₄-V antiferromagnetic superexchange interaction is unchanged.

With decreasing temperature, $\beta\text{-VOSO}_4$ shows a maximum in its magnetic susceptibility, which is attributed to a Néel point $T_N = 25^\circ\text{K}$. Field studies at 4.2°K , 77°K , and room temperature all show a linear dependence to 17.2 kOe .

J. M. Longo
R. J. Arnott
D. A. Batson

Section II

F. CHEMICAL ANALYSIS BY PHOTOMETRIC EDTA TITRATIONS

A method for making automatic photometric titrations with EDTA solutions was described previously.²⁰ It was reported that a Zn-EDTA titration could be performed with a precision of about two parts per thousand. Further investigations have revealed that the Zn-EDTA system is not typical, and that automatic photometric EDTA titrations of other elements are usually more difficult and less precise. However, it has been found that good precision can be achieved by manual titrations.

Photometric data taken manually for Zn-EDTA and Pb-EDTA titrations are shown in Fig. II-10, where the absorbance of the free indicator is plotted against the volume of EDTA solution added. The absorbance rises sharply in the region in which the EDTA is removing the metal ions from the metal-indicator complex, and the correct end point for each curve is the intersection of the two straight-line portions. Under fixed experimental conditions, the slope of the rising straight-line portion approaching the end point depends upon the metal-indicator complex stability, the metal-EDTA complex stability, and the extent of competing reactions. This slope varies from the very steep one shown for Zn-EDTA to the more typical and less steep slope shown for Pb-EDTA, and becomes even less steep for some other elements. The absorbance at the end point depends on the volume of the solution at the end point, which, in turn, depends on the volume of titrant required to react with the element being determined. Since this volume is known only approximately beforehand, there is always some uncertainty in choosing the correct absorbance value for the pre-set end point on the automatic titration equipment. The resulting errors are small when the titration curve is steep but were found to become more significant for less steep curves.

However, it was also found that adding the titrant in small increments, instead of continuously as in the automatic system, and manually making a plot of absorbance versus the volume of titrant added (as in Fig. II-10) gave end points that were reproducible with good precision even when the element concentration was known only within a factor of two or three.

Titration made with 0.01 M solutions and titrant volumes between 2 and 5 ml using the incremental addition-manual plotting technique gave the following relative errors: 0.1 percent for Zn, Pb, and Co; 0.2 percent for Cu; and 0.3 percent for Mg, Ca, and Ba. Thus, this technique retains the advantage of photometric end points²⁰ and gives better precision for more elements than the automatic photometric titration method.

E. B. Owens
Isabel H. Searles

G. MASS SPECTROGRAPHIC ANALYSIS OF FROZEN AQUEOUS SOLUTIONS

The technique of cooling the sample electrodes in spark source mass spectroscopy was first used by Waldron and Wolstenholme²¹ for the analysis of gallium, whose melting point is just above room temperature. Chupakhin and co-workers²² have recently reported preliminary experiments on the application of this method in the analysis of aqueous solutions. The sample electrode was a drop of solution held in a graphite cup, which was connected with flexible metal strips to a cold finger. By filling the cold finger with liquid nitrogen, the solution drop was frozen in situ in the ion source chamber and kept frozen during sparking. We report here an investigation undertaken to further develop the frozen solution technique.

In our first experiments, which were performed with a graphite sample cup and graphite counterelectrode, the photographic plates showed strong lines of carbon and carbon-containing molecules. The intensity ratios of the carbon lines to the oxygen lines and to the lines of the metal elements in the solution fluctuated widely. This precluded the possibility of using the ^{13}C line as an internal standard as Chupakhin had done. When we changed to a nickel sample cup and platinum wire counterelectrode, the carbon lines decreased to trace levels and, contrary to our expectations, the Pt and Ni lines were also very faint. All subsequent experiments were performed in this manner.

The reproducibility of the method was determined by making ten replicate 10^{-10} Coulomb exposures of a frozen drop containing In, Zn, Cu, Ni, Fe, Cr, K, and Cl ions, each present at 0.04 M concentration in very dilute nitric acid solution. The percent transmission values for the line peaks on the photographic plate were measured with a microdensitometer and corrected for plate response and background, to obtain corrected relative exposure values E_c for each line. The ratio $E_c(X)/E_c(\text{Cu})$ in each exposure was calculated for each element. The relative standard deviation from the mean ranges from 8.5 percent for In to 59 percent for Cl, with the average of 21 percent for the elements tested. Chupakhin, et al., report that the relative standard deviation for any element tested was not above 18 percent.

To test the analytical applicability of the method, the same elements were put into three solutions at 0.02, 0.1, and 0.2 M concentrations, and frozen drops were sparked. The $E_c(X)/E_c(\text{Cu})$ ratios plotted against concentration form good analytical curves. The relative standard deviations for each element were calculated at each concentration and averaged over the three concentrations. Values range from 10 percent for Cr to 36 percent for Ni, with an overall average of 18 percent.

The results we have obtained indicate that the method has great potential for determining almost all elements in solution at the 10 ppma level or higher. This is of particular importance for the analysis of solid samples which can be dissolved to form aqueous solutions, because it is usually difficult to obtain solid standards whereas the synthesis of standard solutions is generally easy.

E. B. Owens

REFERENCES

1. Solid State Research Report, Lincoln Laboratory, M. I. T. (1969:1), p. 33, DDC AD-687100.
2. *Ibid.* (1968:4), p. 19, DDC AD-681141, H-909.
3. T. C. Harman, Physics and Chemistry of II-VI Compounds, M. Aven and J. S. Prener, eds. (North-Holland Publishing Co., Amsterdam, 1967), p. 786.
4. A. G. Fischer and W. H. Fonger, Report No. 3 (1965), Contract No. AF 19(628)-3866, U.S. Air Force Cambridge Research Laboratories, Bedford, Massachusetts.
5. Solid State Research Report, Lincoln Laboratory, M. I. T. (1969:3), p. 21, DDC AD-696620.
6. B. M. Kulwicki, "The Phase Equilibria of Some Compound Semiconductors by DTA Calorimetry," Ph. D. Thesis, University of Michigan (1963).
7. V. G. Smith, W. A. Tiller, and J. W. Rutter, *Can. J. Phys.* 33, 723 (1955).
8. H. M. Kasper, *Materials Res. Bull.* 4, 33 (1969), DDC AD-688573; Solid State Research Report, Lincoln Laboratory, M. I. T. (1969:3), p. 26, DDC AD-696620.
9. J. Tudo, *Rev. Chim. minerale* 2, 53 (1965).
10. A. Sieverts and E. L. Müller, *Z. anorg. allg. Chem.* 173, 313 (1928).
11. P. Kierkegaard and J. M. Longo, *Acta Chem. Scand.* 19, 1906 (1965).
12. J. M. Longo and P. Kierkegaard, *Acta Chem. Scand.* 20, 72 (1966).
13. P. Kierkegaard and M. Westerlund, *Acta Chem. Scand.* 18, 2217 (1964).
14. H. A. Eick and L. Kihlberg, *Acta Chem. Scand.* 20, 722 (1966).
15. G. Ladwig, *Z. anorg. allg. Chem.* 364, 225 (1969).
16. C. J. Ballhausen, B. F. Djurinskij, and K. J. Watson, *J. Am. Chem. Soc.* 90, 3305 (1968).
17. International Tables for X-ray Crystallography: Vol. III (Kynoch Press, Birmingham, England, 1962), p. 272.
18. R. A. Edge, *J. Less-Common Metals* 18, 325 (1969).
19. W. B. Doyle, G. McGuire and G. M. Clark, *J. Inorg. Nucl. Chem.* 28, 1185 (1966).
20. Solid State Research Report, Lincoln Laboratory, M. I. T. (1969:3), p. 43, DDC AD-696620.
21. J. D. Waldron and W. A. Wolstenholme, Paper No. 70, Mass Spectrometry Conference, ASTM E-14, New Orleans, June 1962; W. A. Wolstenholme, *Appl. Spectry.* 17, 51 (1963).
22. M. S. Chupakhin, I. A. Kazakov, and O. I. Kryuchkova, *Zh. Anal. Khim.* 24, 3 (1969); M. S. Chupakhin, I. A. Kazakov, O. I. Kryuchkova, and V. P. Frolov, *ibid.*, 24, 165 (1969).

III. PHYSICS OF SOLIDS

A. ELECTRONIC BAND STRUCTURE

1. Interband Magnetoreflexion of α -Sn

The study of interband magnetoreflexion of α -Sn has been completed and a manuscript on this work submitted for publication. As previously reported,¹ several band parameters have been determined quite directly from the experimental data, namely, the Γ_8^+ conduction and valence band masses $m_c^* = 0.028 m$ and $m_v^* = -0.195 m$, respectively, and the $\Gamma_8^+ - \Gamma_7^-$ energy separation $E_g = 0.413$ eV. The s-p interaction parameter $E_p = 24$ eV, the Γ_{25}^+ spin-orbit splitting $\Delta = 0.80$ eV, and the masses $m^*(\Gamma_7^-) = -0.058 m$ and $m^*(\Gamma_7^+) = -0.04 m$ are found less directly.

A puzzling feature of the theoretical fit to the data is the systematic deviation at high photon energies for the Γ_8^+ valence-band to Γ_8^+ conduction-band transitions. These transitions, across the zero energy gap, are first detected at $h\nu \approx 0.04$ eV, due to instrument limitations, and are followed up to $h\nu \approx 0.6$ eV. The fit of the theory is quite acceptable below about 0.2 eV but deteriorates above this energy, as is shown in Fig. III-1 which covers the range 0.2 to 0.4 eV for one component of circular polarization. With the idea that the unexplained curvature results from the interaction of the Γ_{15} bands ($\Gamma_8^- + \Gamma_6^-$ double group) with Γ_8^+ , we have extended the effective mass theory to include the Γ_{15} bands as part of the basis of the matrix Hamiltonian. The effect of this is to include the interaction between Γ_{15} and Γ_8^+ exactly rather than just to order k^2 , as done previously.

Recent OPW band calculations² place the Γ_8^- and Γ_6^- levels 2.43 eV and 1.95 eV, respectively, above Γ_8^+ . We find that these are too high to cause a noticeable correction to the theoretical curves of Fig. III-1; it is necessary to shift these to less than 1 eV to begin to get the right size of correction. Because the lower of the spin-orbit split Γ_{15} bands (Γ_6^-) has a larger mass than the Γ_8^+ conduction band, these bands try to cross at small E and k values. Actually, these bands can cross only along $\langle 100 \rangle$ directions, and for other directions the bands repel each other,

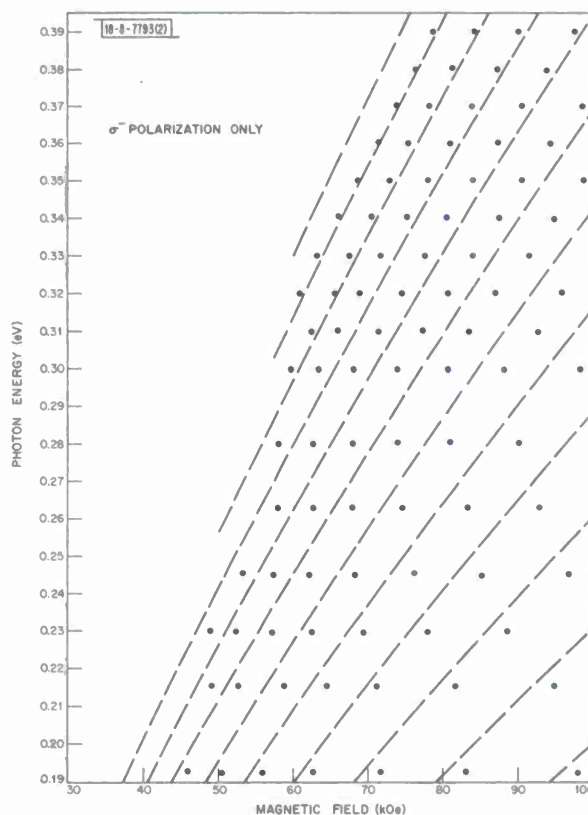


Fig. III-1. High-energy segment of the $\Gamma_8^+ \rightarrow \Gamma_8^+$ transition spectrum showing systematic discrepancy between theory and experiment.

Section III

as shown in Fig. III-2. However, the admixture of the Γ_7^- basis function in the Γ_8^+ conduction band, which makes the Γ_8^+ valence-band to Γ_8^+ conduction-band optical transitions possible,

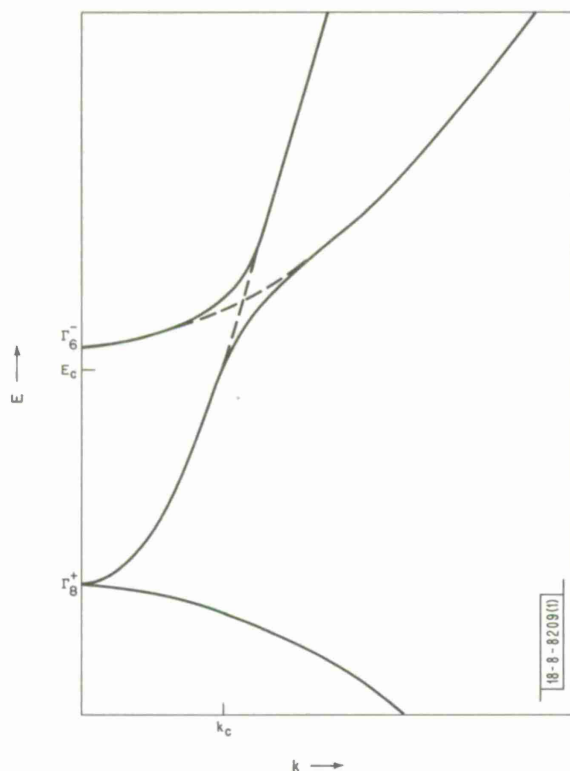


Fig. III-2. Modified band structure which qualitatively accounts for anomalous features of magnetoreflexion and magnetoresistance experiment. Here, k_c corresponds to Fermi radius of a sphere holding $\approx 5 \times 10^{17}$ electrons/cm³ and $E_c = 0.1$ eV.

Another problem which arises is the sign of the parameter G , which specifies the $\Gamma_{12} - \Gamma_{25}^1 \vec{k} \cdot \vec{p}$ interaction. For other diamond and zincblende materials, G is less than zero, indicating that the predominant interaction comes from a Γ_{12} conduction band. The size and sign of G can be specified from the conduction-band anisotropy⁵ and the valence-band effective mass, if the $\Gamma_{15} - \Gamma_8^+$ interaction is known. Taking the position of the Γ_{15} bands from the band structure OPW calculations, we find that G is positive, which would indicate that a Γ_{12} valence band makes the predominant contribution. However, if the band structure of Fig. III-2 is assumed, with the Γ_{15} bands less than 1 eV above Γ_8^+ , G is negative as found with the other semiconductors. These problems are discussed more fully in the submitted manuscript.

transfers to the upper conduction band above the energy E_c in Fig. III-2, and the final state of the optical transitions shifts from the Γ_8^+ to the Γ_6^- band.

In our magnetoreflexion experiments, we did not observe direct experimental evidence of the band structure shown in Fig. III-2, such as extra transitions or strong magnetic-field dependent intensities. However, the large photon energy interval between the experimental points may be the reason for this. The band crossing scheme is attractive for explaining the conduction-band mass vs electron concentration behavior reported by Booth and Ewald from oscillatory magnetoresistance experiments.³ They observe a marked change in m_c^* vs n dependence at $n \approx 5 \times 10^{15}$ cm⁻³, which is in qualitative agreement with that predicted from Fig. III-2.

If the band structure of Fig. III-2 is discarded, i.e., one retains the Γ_{15} bands at ≈ 2 eV above Γ_8^+ , then we must attribute the theoretical experiment discrepancies in Fig. III-1 to the breakdown of the various simplifying assumptions behind the $\vec{k} \cdot \vec{p}$ and magnetic-field-effective-mass Hamiltonians. Apparently this would be a unique situation for the diamond-zincblende lattice semiconductors.⁴

S. H. Groves A. W. Ewald[†]
C. R. Pidgeon[‡] R. J. Wagner[‡]

[†] Francis Bitter National Magnet Laboratory, M.I.T.

[‡] Northwestern University, Evanston, Illinois.

2. Effects of Applied Stress on Phosphorus-Doped Silicon

Low-temperature measurements of the energy shift with stress of transitions from the ground level to excited p-like levels of phosphorus atoms in silicon, made earlier⁶ with applied stresses up to 6×10^8 dynes/cm², have now been extended to 17.5×10^8 dynes/cm². To do this, a new sample holder was built which accommodates samples with a length-to-thickness ratio of 10:1 instead of the 1:1 ratio previously used. The use of a long, thin sample leads to a considerably more homogeneous stress than is obtained with the square samples used before. The resulting improvement in the spectra is quite dramatic.

The results for a stress applied along a [001] crystal axis are shown in Fig. III-3 where it is seen that a nonlinear energy shift of the transition energies in an upward direction becomes

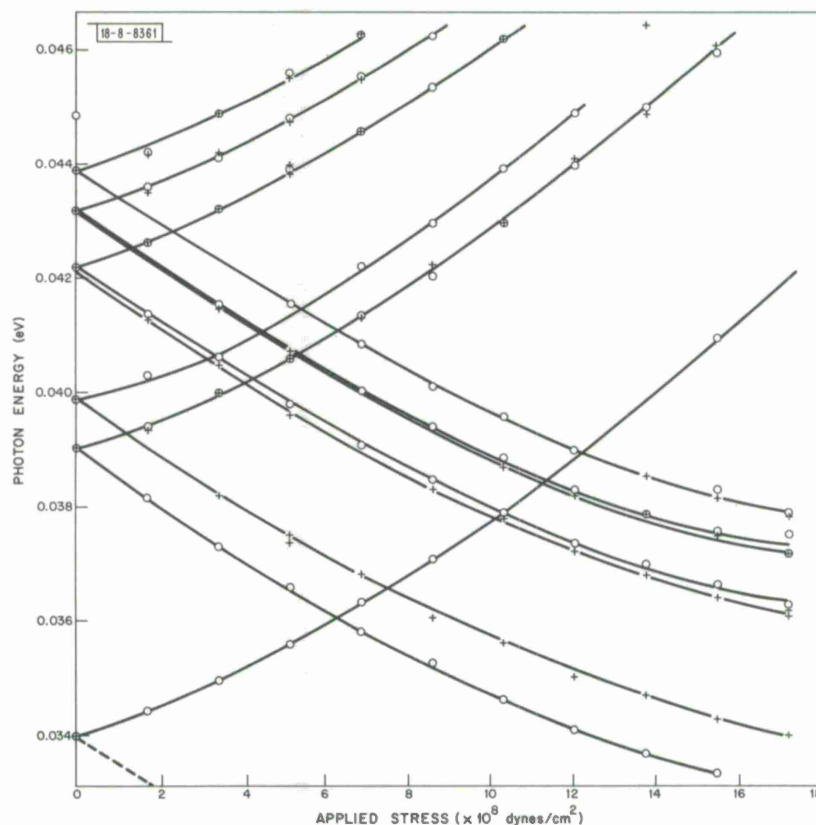


Fig. III-3. Effect of applied uniaxial stress on transition energies of phosphorus in silicon. Applied stress is parallel to [001] crystal axis.

very apparent for applied stresses above 6×10^8 dynes/cm². This upward shift can, with good accuracy, be accounted for by the downward shift with stress of the ground level which we have calculated, following Feher and Wilson,⁷ using effective mass and deformation potential theory and taking account of intervalley coupling of the 1s-like states.

W. E. Krag
W. H. Kleiner
H. J. Zeiger

3. Silicon Conduction-Band Deformation Potential and Donor Dipolar Hyperfine Coupling

The shear deformation potential coefficient⁸⁻¹⁰ D_s of the conduction-band edge of silicon has been found from photoexcitation experiments¹¹⁻¹³ on donors to have the value 7.9 eV. This is in striking disagreement with values (presumed accurate to within about 6 percent) obtained earlier from electron spin resonance (ESR) experiments on donors by Wilson and Feher¹⁴ (W-F); these values range from about 10 to 11 eV, depending on the donor. The photoexcitation value is expected to be reliable, since it is derived directly from the observed relative shift with strain of p-like excited donor levels and is donor independent. This indicates that the difficulty lies in the ESR values, which are derived from the observed strain dependence of the hyperfine splitting due to the donor nucleus. The W-F treatment was based on the contact hyperfine interaction. The dipolar hyperfine interaction was apparently not considered.

Here we show that the discrepancy between the values of D_s cannot reasonably be attributed simply to neglect of the dipolar hyperfine coupling. Using the effective mass theory of Luttinger and Kohn and deformation potential theory, W-F treat the effect of strain as a perturbation which mixes a wave function ψ_1 of the $1s(E)$ level with the ground $1s(A_1)$ wave function ψ_0 : $\psi = c_0\psi_0 + c_1\psi_1$. This is used to calculate the expectation value of the hyperfine interaction K_{hf} . We proceed in the same way, but include the dipolar hyperfine coupling in K_{hf} . The ratio \mathcal{R} of the hyperfine splitting for a given strain to its value in the absence of strain, the observed quantity, then takes the form

$$\mathcal{R} = c_0^2 + Ac_0c_1 + Bc_1^2 \quad (1)$$

where A and B are independent of strain and vanish in the absence of the dipolar interaction, which is the case considered by W-F. A and B depend on the angle Θ between the uniaxial strain axis and the magnetic-field direction according to

$$\begin{aligned} A &= (3 \cos^2 \Theta - 1) a \\ B &= (3 \cos^2 \Theta - 1) b \end{aligned} \quad (2)$$

where

$$a = \frac{9}{8\pi} \frac{\langle \psi_0 | W | \psi_1 \rangle}{\langle \psi_0 | \delta(\vec{r}) | \psi_0 \rangle} \quad b = \frac{9}{8\pi} \frac{\langle \psi_1 | W | \psi_1 \rangle}{\langle \psi_0 | \delta(\vec{r}) | \psi_0 \rangle} \quad (3)$$

In the matrix elements, $\delta(\vec{r})$ is the Dirac delta function, $W = r^{-3} [1 - 3(z/r)^2]$ with the uniaxial strain along the z -axis, and ψ_1 transforms as $3z^2 - r^2$ under the tetrahedral point group T_d . The following two arguments indicate that a and b are, in fact, negligible.

The two matrix elements of W , which are not required by symmetry to be zero, can be estimated on the basis of tight-binding Bloch functions if it is assumed that the dominant contribution comes from the central cell region of the donor. Both matrix elements of W are zero in this approximation which was used successfully to predict¹⁵ the order in energy of the three observed¹⁶⁻¹⁸ $1s$ -like levels (the A_1 , E , and T_2 levels) of silicon donors.

Figure III-4 shows \mathcal{R} as a function of the W-F strain parameter $x = D_s s' / E_{12}$, where E_{12} is the energy separation between the $1s$ -like A_1 and E levels, and $s' = 2(s_{11} - s_{12}) T$; s_{11} and

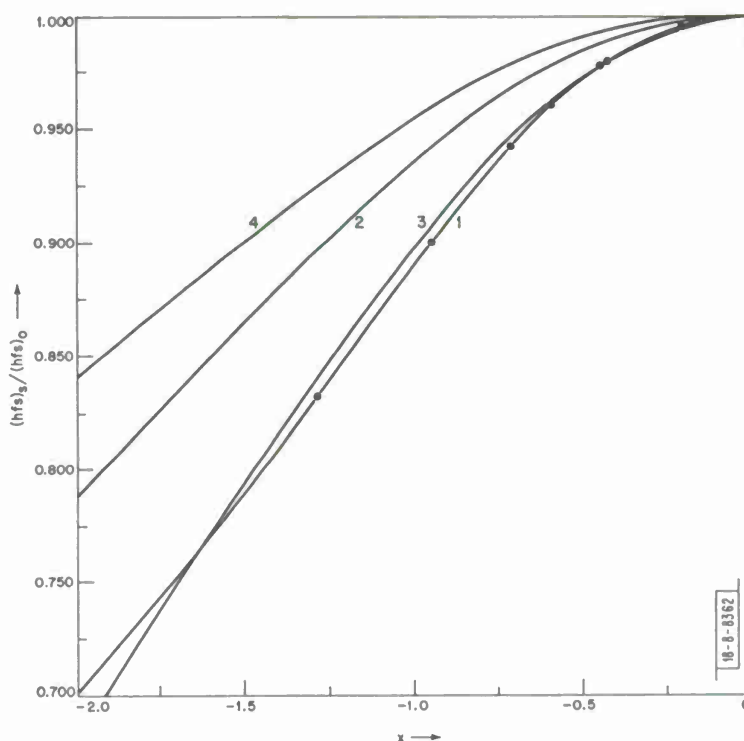


Fig. III-4. Hyperfine splitting of silicon donor ESR line as a function of strain: observed, curve 1; predicted, curves 2, 3, and 4.

s_{12} are standard elastic compliance coefficients, and T is the uniaxial stress. The value $D_s = 7.9$ eV from the photoexcitation experiments is used. Curve 1 represents the experimental data; curves 2, 3, and 4 show predictions based on the above treatment. Curve 2 neglects dipolar hyperfine coupling ($A = B = 0$). The difference between curves 1 and 2 shows the discrepancy which is to be explained. A reasonably good fit to curve 1 can be obtained by choosing A and B near the line $A/(-0.20) + B/(-0.45) = 1$ in the A - B plane and in or near the third quadrant. As an example, curve 3, which fits the data satisfactorily, is for $A = -0.05$ and $B = -0.40$. To make the corresponding $|a|$ and $|b|$ as small as possible, suppose curve 3 is for $\Theta = 0$, so that $a = A/2$ and $b = B/2$. These values of a and b give curve 4 when $\Theta = \pi/2$, in which case $A = 0.025$, $B = 0.20$. The difference between curves 3 and 4 is large enough to be easily observed experimentally. We conclude that dipolar hyperfine coupling of the electron spin to the donor nucleus large enough to account for the discrepancy between the photoexcitation and ESR values of D_s would entail an easily detectable dependence of the hyperfine splitting on the magnetic-field direction – an anisotropy not mentioned by W-F, and therefore presumably not observed.

W. H. Kleiner

4. Shubnikov-de Haas Measurements in $\text{Pb}_{1-x}\text{Sn}_x\text{Te}$ Under Hydrostatic Pressure

In $\text{Pb}_{1-x}\text{Sn}_x\text{Te}$, the energy gap (at 4.2°K) is believed to decrease with increasing Sn content from 0.19 eV at $x = 0$ to zero at $x = 0.35$. In this composition range, it decreases also with

Section III

pressure. The oscillatory magnetoresistance (Shubnikov-de Haas effect) has been observed up to pressures of 8 kbars on samples with $0.16 \leq x \leq 0.32$. The Fermi surface shape appears not to change with pressure, but is still composed of prolate ellipsoids along the [111] axis at the L points. (This measurement is somewhat obscured by nonhydrostatic strain components which are sometimes introduced in the solidification of the helium used to transmit the pressure. Nevertheless, any systematic change of the Fermi surface cross-sectional areas greater than 5 percent would have been detected in going from 0 to 8 kbars.) The cyclotron effective masses at the Fermi level, deduced from the temperature dependence of the resistance oscillation amplitudes, decrease with pressure, as shown in Fig. III-5.

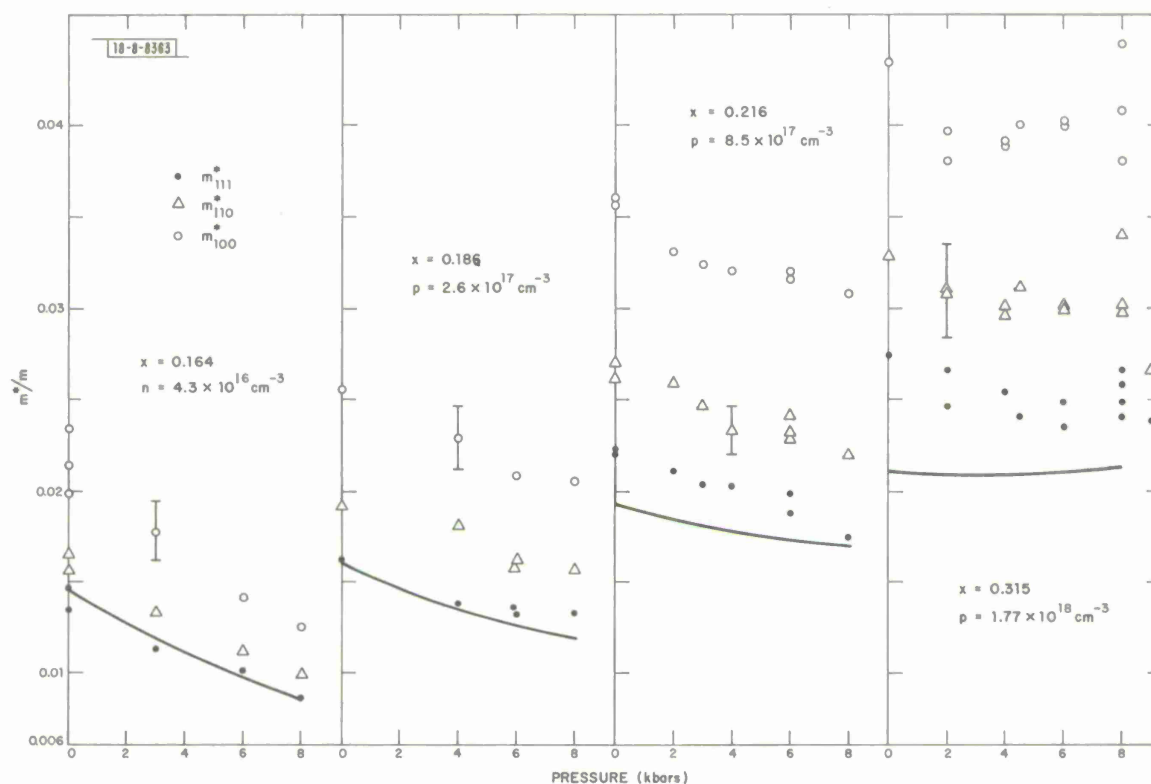


Fig. III-5. Cyclotron effective masses [$m^* = (\hbar^2/2\pi)(\partial A_{\perp}/\partial E_F)$, where A_{\perp} is cross-sectional area of Fermi surface perpendicular to magnetic field, and E_F is Fermi energy] as a function of pressure in $\text{Pb}_{1-x}\text{Sn}_x\text{Te}$, for one n- and three p-type samples. Solid lines show behavior expected for m_{111}^*/m from two-band model. For magnetic field in [111] and [110] directions, masses shown correspond to smaller cross-sectional areas.

On the basis of the two-band model,¹⁹ the following approximate expression can be derived²⁰ for the transverse (111) cyclotron mass of either holes or electrons:

$$\frac{m_{111}}{m} = \left[\left(\frac{E_g}{E_p} \right)^2 + \frac{8\mu_B \alpha}{E_p} \right]^{1/2} \quad (4)$$

where E_g is the gap, $E_p = 2P_{\perp}^2/m$ (P_{\perp} is a $\vec{k} \cdot \vec{p}$ matrix element parameter¹⁹), m is the free electron mass, μ_B is the Bohr magneton, and α is the S.dH. (111) frequency (in gauss). If

the dependence of E_g (in eV) on composition x , and on pressure P (in kbars) is given by $E_g = 0.19 - 0.19(x/0.35) - 0.0075P$ where the constant 0.0075 eV/kbar is assumed to be the same as in PbTe ,²¹ then the only adjustable parameter in Eq. (4) is E_p . With $E_p = 8.0 \text{ eV}$ chosen to fit m_{111}^* at $P = 0$ for the lowest carrier concentration p-type sample, we obtain the solid lines in Fig. III-5. Equation (4) is seen to predict within the accuracy of the measurements the dependence of m_{111}^* on pressure for the lower concentration samples. For the higher concentration samples, a smaller value of E_p would produce agreement.

We have also measured the resistivity of the samples as a function of pressure. For the 31.5-percent SnTe sample, measurements of resistivity were extended to 10 kbars at 77°K . A minimum was found at 9 kbars, possibly indicating the crossing of the bands.²¹ For the other samples, the resistivity decreases with pressure at both 77° and 300°K .

J. Melngailis W. C. Kernan
J. A. Kafalas T. W. Hilton
T. C. Harman

B. MAGNETISM

1. Magnetic Ordering Effects on Ultraviolet Reflectance of EuS and EuSe

Previous studies of magnetic ordering effects in the low-energy reflectance of the magnetic semiconductors EuO , EuS , and EuSe (Ref. 22) have provided direct evidence that the conduction band is spin-polarized in the ferromagnetic state and that the low-energy peak E_1 is due to $4f^7 \rightarrow 4f^6 5d(t_{2g})$ transitions. We have now made measurements of the effects of magnetic ordering on the E_2 reflectance peak near 4 eV in EuS and EuSe which suggest that the E_2 peak is due at least in part to $4f^7 \rightarrow 4f^6 5d(e_g)$ transitions.

The effect of magnetic ordering on the E_2 reflectance peak in single-crystal EuS and EuSe was measured in a domain orienting magnetic field of 40 kOe using circularly polarized light in the Faraday configuration ($E \perp H$) at near-normal incidence at 1.5°K . At this temperature, both EuS and EuSe are ferromagnetic.^{23,24} Figure III-6 shows the polarized E_2 reflectance of EuS and EuSe as well as E_1 for comparison. In EuS , the lower energy portion of E_2 is predominantly σ_R , and the higher energy portion is σ_L . In EuSe , the lower energy portion of E_2 is an almost equal mixture of σ_R and σ_L , while the higher energy portion is predominantly σ_L again. It is noteworthy that in

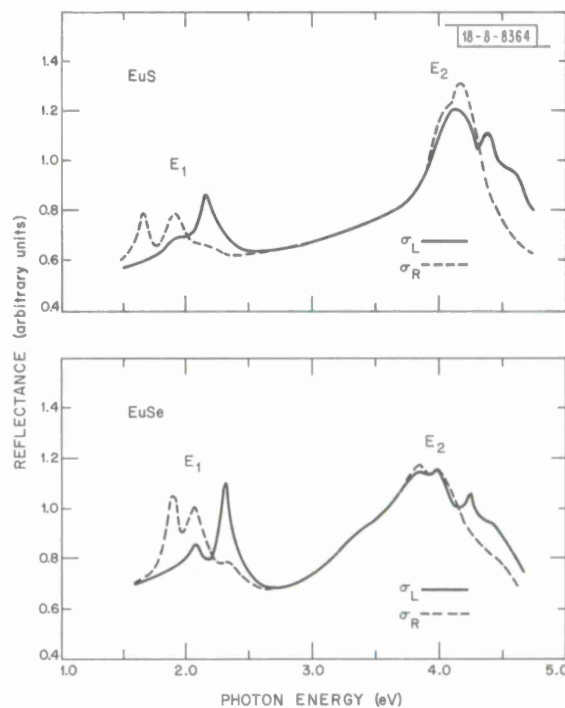


Fig. III-6. Reflectance of EuS and EuSe at 1.5°K at near-normal incidence using right (σ_R) and left (σ_L) circularly polarized light in 40-kOe field, $E \perp H$.

EuSe a very similar curve is obtained even at 20°K, demonstrating that magnetic ordering exists well above T_c . As shown in Fig. III-6, the σ_R dominance on the low-energy side of E_1 is much more pronounced than that of E_2 .

As we have previously argued regarding the E_1 peak,²² the existence of polarization dependence and structure in E_2 at temperatures both below and above T_c in an orienting magnetic field indicates that the E_2 structure involves transitions from the $4f^7(^8S_{7/2})$ localized ground state, presumably in this case to the $4f^6(^7F_J)5d(e_g)$ excited state configuration.

As we have noted, there is no change in the polarization dependence of E_2 as T decreases below T_c in EuSe, which is in contrast to E_1 where changes do occur. However, this behavior is consistent with assigning E_2 to $4f^7 \rightarrow 4f^6 5d(e_g)$ transitions and E_1 to $4f^7 \rightarrow 4f^6 5d(t_{2g})$ transitions. The difference between the E_1 and E_2 polarization behavior can be explained by the fact that the $5d(t_{2g})$ band is split by spin-orbit coupling whereas the $5d(e_g)$ band is not, at least at $\vec{k} = 0$. Below T_c , the e_g band becomes exchange split into pure spin-up and pure spin-down components, in contrast to the t_{2g} band where the spin states are mixed by spin-orbit coupling. Transitions from the spin-down $4f^7(^8S_{7/2})$ ground state to the pure spin-up component of the $5d(e_g)$ band are not allowed by electric dipole interaction so that no splitting should be observed. Consequently, the polarization dependence of E_2 should not change drastically at T_c , since transitions to only one of the exchange split bands are allowed, in agreement with our observations. Since the magnetization increases as T decreases, we could expect intensity changes in σ_R and σ_L below T_c , but our results show only small effects. Additional discussion concerning this interpretation can be found elsewhere.^{25,26}

W. J. Scouler J. O. Dimmock
J. Feinleib C. R. Pidgeon†

2. Magneto-optical Effect of Field-Induced Spin Alignment in Antiferromagnetic EuTe

In the preceding report (1969:3, p. 48, DDC AD-696620), the effects of magnetic ordering on the reflectance of ferromagnetic EuS and EuSe were discussed. Similar measurements have been made on EuTe which has been shown to be an antiferromagnet with a Néel temperature $T_N \approx 10^\circ\text{K}$ (Ref. 27). Our measurements of the polarized reflectance of single-crystal EuTe show strongly field-dependent effects. Figure III-7 shows the reflectance at 1.5°K for $H = 0$ and 97.4 kOe; the peak positions and polarization as a function of applied magnetic field are shown in the lower half of the figure. As the magnetic field is increased, the structure for $H = 0$ (where there is no polarization dependence) gradually shifts to that seen at 97.4 kOe, the effects saturating around to 80 kOe. The polarized structure characteristically seen for E_1 in EuO, EuS, and EuSe (Ref. 22) appears when the field exceeds 60 kOe. The fact that the E_1 structure of EuTe in high fields has a form identical to that of E_1 in ferromagnetic EuO, EuS, and EuSe, where the structure has been identified with exchange splitting of the conduction band by ferromagnetic ordering, indicates that a field-induced spin alignment has been obtained in EuTe.

E_2 at low fields at 1.5°K has a doublet structure with a separation of 0.45 eV between peaks, the largest separation in the europium chalcogenide series. As the field increases, a third middle peak appears and all three shift and split into σ_R and σ_L components, the effects again saturating around 80 kOe, as shown in the lower portion of Fig. III-7.

† Francis Bitter National Magnet Laboratory, M.I.T.

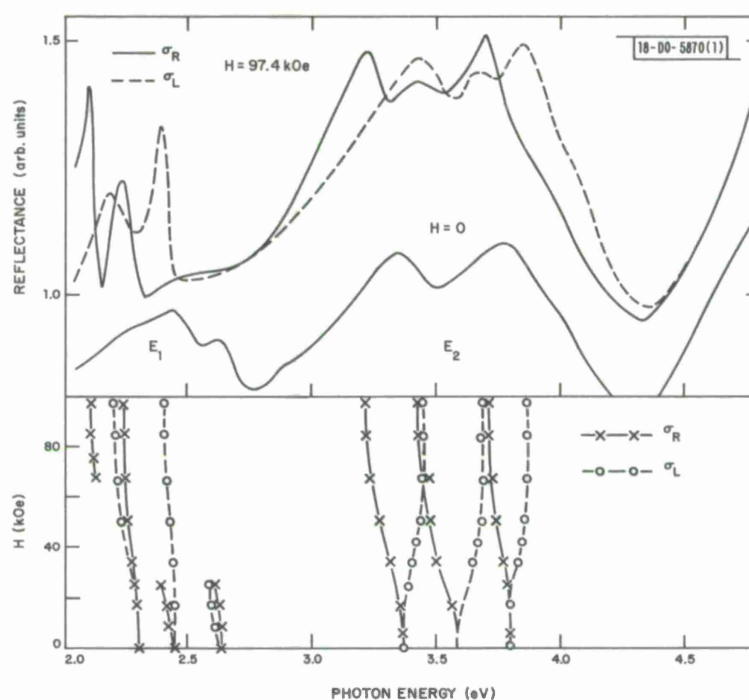


Fig. III-7. Reflectance of EuTe at 1.5°K at near-normal incidence using right (σ_R) and left (σ_L) circularly polarized light for $H = 0$ and 97.4 kOe. The $H = 0$ curve has been shifted for clarity. Lower portion shows position of E_1 and E_2 multiplet peaks as function of H .

The results for antiferromagnetic EuTe indicate that the final conduction-band state may be split below T_N , but the exchange interaction is more complex than in the ferromagnetic case. In the antiferromagnetic case, the $5d(t_{2g})$ and $5d(e_g)$ bands are perturbed by the alternating-spin superlattice of the $4f$ electrons on the Eu^{2+} ion. The perturbation can best be described by the introduction of new superzone boundaries which divide the Brillouin zone. On these superzone boundaries, each d-band is split into two components: (a) a lower energy component in which the spin-wave functions alternate in order to be aligned with the $4f$ electrons on each site, and (b) a higher energy component in which the spin-wave functions are oppositely aligned. However, since each band component has both up- and down-spin parts, we expect no polarization dependence at low (< 30 kOe) fields, in accordance with our results. In addition to this antiferromagnetic superlattice band splitting, the magnetic field induces a net ferromagnetic interaction. This occurs above the spin flop field of about 4 kOe (Ref. 28), when the sublattice magnetizations are perpendicular to the magnetic field and then slowly cant up toward the direction of the magnetic field. The change in the structure of the reflectance spectrum with increasing applied magnetic field can be explained in terms of the gradual removal of the antiferromagnetic superzone boundaries and the introduction of the usual band splitting as the spin structure becomes ferromagnetic. From considerations discussed elsewhere,²⁹ the calculated saturation field H_s required for spin alignment is about 70 kOe, in reasonable agreement with the 80-kOe saturation observed in our magneto-optical data.

Section III

The magneto-optical data for EuTe can thus be understood in terms of our earlier model for EuO, EuS, and EuSe with modifications introduced because of the EuTe antiferromagnetic behavior.

J. Feinleib
C. R. Pidgeon†

3. Magnetic Properties of Cr₅S₆

Cr₅S₆ is a high-conductivity material which becomes ferrimagnetic at about 305°K and undergoes a ferrimagnetic-antiferromagnetic transition at T_t (150° to 160°K). It has a NiAs structure with ordered vacancies,³⁰ and van Laar³¹ has found by neutron diffraction that the low-temperature transition is from a collinear Néel-type ferrimagnet above T_t to a spiral configuration below T_t. B. van Laar observed a smooth and continuous variation of the wave vector k characterizing the spiral from well below T_t to zero at and above T_t, indicative of a second-order phase change, which is at variance with the significant hysteresis in T_t depending on whether it is observed during a cooling or warming cycle.^{32,33}

To gain further insight into the magnetic behavior of Cr₅S₆, we have undertaken a study of its magnetic properties as a function of pressure as well as of magnetic field and temperature. We have also applied the generalized Luttinger-Tisza method (GLT)³⁴ to establish boundary conditions for the magnetic interactions to be consistent with the observed spin configuration.

The hysteresis effect of T_t was observed and found to be essentially independent of pressure. The magnetic-field dependence of T_t was found to be essentially constant between 0 < H < 6 kOe and 9 < H < 12 kOe with values of (ΔT_t/ΔH) equal to -0.64°/kOe and -0.45°/kOe, respectively, with a smoothly curving nonlinear relationship at the intermediate fields. The value obtained between 9 and 12 kOe is in excellent accord with the value -0.437°/kOe obtained at high pulsed fields by Flippen and Darnell³⁵ in CrS_{1.17}. The variations of both the Curie point T_c and T_t were linear with pressure, yielding values of ∂T_c/∂P = -2.83°K/kbar and ∂T_c/∂P = +0.04°K/kbar. The former value is in reasonable accord with the value -2.6°K/kbar obtained by Kamigaichi, *et al.*,³⁶ for CrS_{1.17} on the basis of conductivity measurements, but the latter disagrees sharply with their value ∂T_t/∂P = -3.5°K/kbar. Assuming a first-order transition, the small change we observe is in accord with the failure to observe a significant volume change of the crystal through the transition temperature.³⁷

In addition, the application of pressure was found to reduce the net magnetization throughout the ferrimagnetic range, as shown in Fig. III-8(a) which gives the temperature variation of the magnetic moment in a field of 8 kOe at atmospheric pressure and 5 kbars. The observed change can be due to the effect of pressure on T_c, or on the intrinsic moment of the ions, or both. The relative contributions of these terms is given by the thermodynamic relationship

$$\frac{1}{\sigma} \left(\frac{\partial \sigma}{\partial P} \right)_{H, T} = \frac{\frac{1}{\sigma_0} \left(\frac{\partial \sigma_0}{\partial P} \right)_{H, T} - \frac{1}{\sigma} \left(\frac{\partial \sigma}{\partial T} \right)_{P, H} \frac{T}{T_c} \left(\frac{\partial T_c}{\partial P} \right)}{1 + \frac{3\alpha}{\kappa} \frac{T}{T_c} \left(\frac{\partial T_c}{\partial P} \right)} \quad (5)$$

† Francis Bitter National Magnet Laboratory, M.I.T.

where σ is the saturation moment at temperature T , σ_0 is the saturation moment at 0°K , α and κ are the thermal expansion coefficient and compressibility, respectively. Substitution of experimentally determined values for $T = 195^\circ\text{K}$ into Eq. (5) leads to the result

$$\frac{1}{\sigma_0} \left(\frac{\partial \sigma_0}{\partial P} \right)_{H, T} = -0.011 + \frac{0.059 \alpha}{\kappa} \quad (6)$$

Taking 10^{-2} as a reasonable upper limit for α/κ , we are led to the conclusion that almost two-thirds of the observed magnetization decrease of 0.017 is due to changes in the intrinsic net moment.

Equation (5) assumes that

$$\sigma/\sigma_0 = f(T/T_c) \quad (7)$$

independent of pressure. That this is true for our sample is indicated by Fig. III-8(b), where the two curves of Fig. III-8(a) have been normalized relative to each other. (The magnetization scales were normalized relative to each other by equating the magnetization of the two curves at the single point $T/T_c = 0.656$.)

The variation of moment with pressure and van Laar's observation of approximately equal but nonintegral moments at the various chromium sites are not phenomena normally associated with ionic models. Although variation in spin-orbit mixing of nearly degenerate up- and down-spin levels might account satisfactorily for these phenomena within a localized model, the collective-electron explanation in terms of slight shifts between nearly degenerate up- and down-spin bands would appear more natural. In addition, the collective model is consistent with the observation of metal-like conductivity in Cr_5S_6 (Ref. 38).

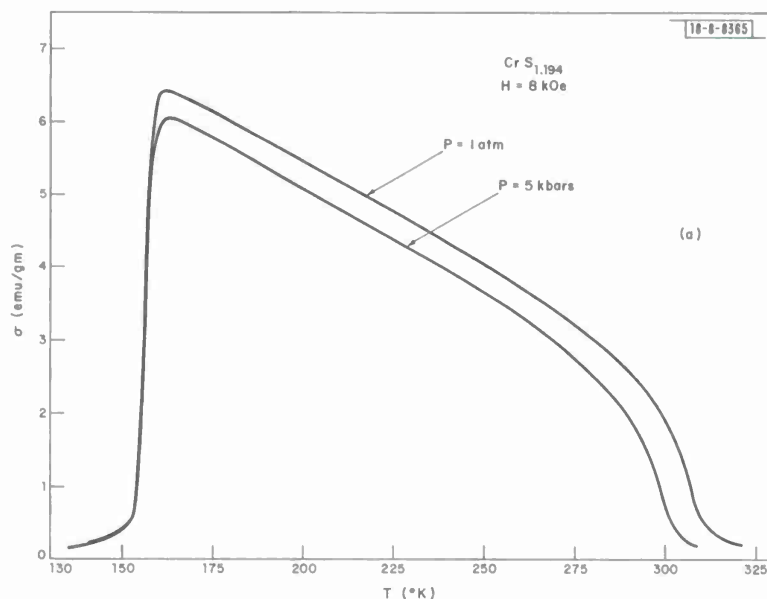


Fig. III-8(a). Experimental results of variation of magnetic moment with temperature of $\text{CrS}_{1.194}$ at atmospheric pressure and 5 kbars.

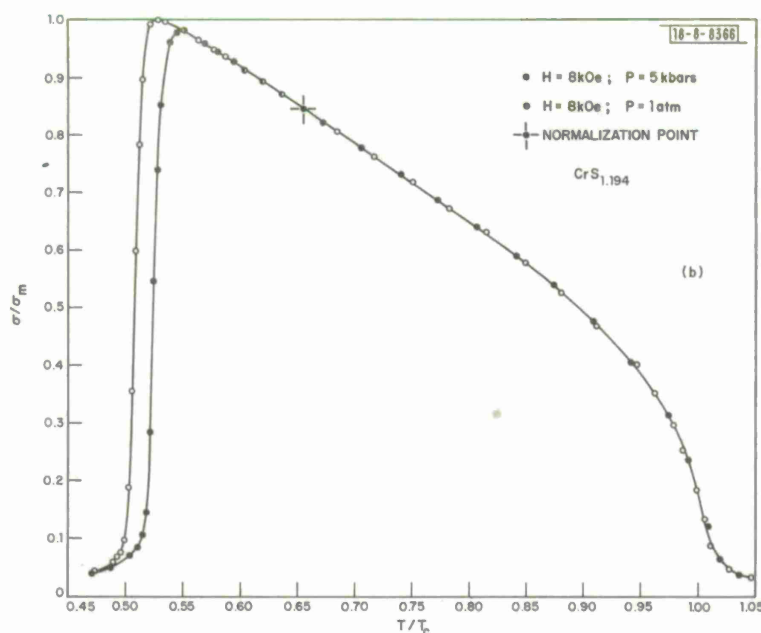


Fig. III-8(b). Curves of Fig. III-8(a) with horizontal axes normalized to individual Curie points and vertical axes normalized to maximum magnetic moment value at 1 atm (σ_m). Magnetic moment of 5-kbar curve was normalized by setting it equal to that of atmospheric pressure curve at $T = 0.656 T_c$.

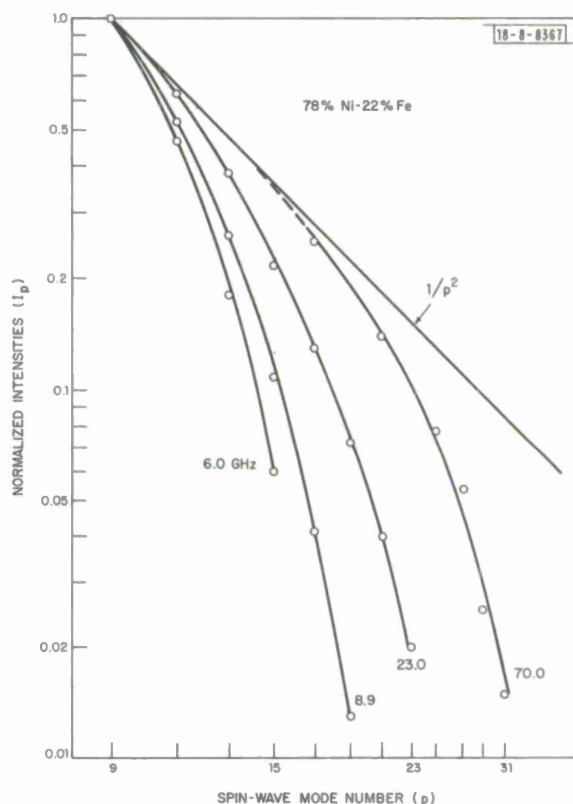
A study of the classical ground state in Cr_5S_6 has been started involving determination of the spin configuration which minimizes the Heisenberg exchange energy. Although the validity of the Heisenberg Hamiltonian is questionable in a high-conductivity material, it has proved fruitful in other such materials. We have been able to obtain sets of interactions for which the van Laar spiral is stable at $T = 0^\circ\text{K}$ and which is unstable relative to the Néel-type ferrimagnetic configuration at the Curie temperature. This suggests that the primary driving mechanism of the transition can be explained by the change in relative stability of the two states as a function of thermal fluctuations, with no need to introduce additional assumptions such as temperature variation of the interaction parameters. This would agree with the gradual change in the wave vector \underline{k} as observed by van Laar. However, at the temperature at which the energy of the two configurations is equal, magneto-elastic effects can cause the transition to be of first order.

N. Menyuk
K. Dwight
J. A. Kafalas

4. Intensities of Spin-Wave Resonance Modes in Thin Films

Measurements have been made of the intensities of the spin-wave absorption peaks of two nickel-iron films of differing compositions and thicknesses from 5 to 70 GHz using stripline and cavity techniques. It has been found that the intensities are a strong function of frequency. Since similar results were obtained for both films, the data of just one of the films are presented in Fig. III-9.

Fig. III-9. Experimental normalized intensities of spin-wave resonances as a function of mode index number p with RF frequency as a parameter. Film thickness was 5000 Å, with $4\pi M = 10.9$ kOe, $g = 2.1$, and $A = 0.9 \times 10^{-6}$ erg/cm. Data were taken at room temperature. (Qualitatively similar data were obtained for 63%Ni-37%Fe film of thickness 5670 Å, with $4\pi M = 14.0$ kOe from 5.0 to 70 GHz.)



The relative intensities were measured between the maxima and minima of first-derivative traces of the spectra. At each frequency, the intensities were normalized to the $p = 9$ mode. This mode was chosen to be the starting point for the normalization because the modes with lower p -numbers were distorted by the envelope of the principal mode.

The results indicate that the spin-wave dispersion is quadratic in mode number from $p = 9$ to $p = 21$, and that the normalized intensity behavior of the resonances is not $1/p^2$ but approaches $(1/p)^8$ to $(1/p)^{11}$. Since the assignment of the mode numbers was unambiguous for these films, the odd-integer numbering scheme (and surface spin pinning) cannot be invalidated simply on the basis that the intensities deviate from $1/p^2$ behavior.³⁹

More generally, the strong frequency dependence of the intensities dictates that any intensity model for thin films, to be meaningful, must take such behavior into account. All presently proposed intensity models fail in this respect.

R. Weber
P. E. Tannenwald
C. H. Bajorek

Sections 5 and 6 below are abstracts of papers presented at the Fifteenth Annual Conference on Magnetism and Magnetic Materials, Philadelphia, Pennsylvania, 18-21 November 1969.

5. "Theory of Localized vs. Band Magnetic Semiconductors

"We have considered the question of whether the Hubbard Hamiltonian can lead to properties characteristic of two types of semiconductors, depending on the value of the ratio Δ/I of bandwidth to intra-atomic Coulomb integral. In one type there is a transformation, with increasing T , from a magnetic insulating state to a paramagnetic insulating state, and in the other the system goes from a magnetic insulating state to a paramagnetic metallic state. We have applied a new variational single-determinantal approximation which, in contrast to the standard thermal Hartree-Fock approximation, duplicates the exact behavior of the model both in the atomic limit, $\Delta/I = 0$, and the band limit $\Delta/I = \infty$. Limiting ourselves to well-known types of one-electron states, we have obtained stability boundaries (as determined by the free energy) between various phases."

T. A. Kaplan
R. A. Bari

6. "Eigenvalue Degeneracy as a Possible Mathematical Mechanism for Phase Transitions

"Some years ago Ashkin and Lamb noted that the phase transition in the two-dimensional Ising model with nearest-neighbor interaction was characterized mathematically by an asymptotic degeneracy of the largest eigenvalue of a linear operator. More recently Kac and Thompson showed this eigenvalue degeneracy also characterized the phase transition in the Kac model (with weak, long-range forces), suggesting that this "mathematical mechanism" is not restricted to systems with short-range forces. However both the Kac model and the Ising model consider the "spins" to be one-dimensional unit vectors assuming only the discrete values $+1$ and -1 . We are therefore led to consider the nature of the phase transition in one of the few exactly-soluble models in which the spins can assume an entire continuum of orientations – the linear chain of classical spins of arbitrary spin dimensionality interacting isotropically through the Hamiltonian

$$H_\nu = \sum_{i=1}^N J_{i,i+1} S_i^{(\nu)} S_{i+1}^{(\nu)},$$
 where the exchange constants $J_{i,i+1}$ are arbitrary numbers. We find for all spin dimensionalities ν that the two-spin correlation function may be expressed as $\rho_N(r) = (\lambda_1/\lambda_0)^r$, where λ_0 and λ_1 are the largest and next-largest eigenvalues of a certain linear operator. Thus the onset of long-range order, $\lim_{r \rightarrow \infty} \rho_N(r) \neq 0$, is characterized by the degeneracy of λ_0 and λ_1 ."

H. E. Stanley
Koichiro Matsuno[†]
Sava Milosevic[†]

[†] Physics Department, M.I.T.

C. LASER SCATTERING

Section 1 below is an abstract of a paper presented at the Fifteenth Annual Conference on Magnetism and Magnetic Materials, Philadelphia, Pennsylvania, 18-21 November 1969.

1. "Two-Magnon Raman Scattering in KNiF_3

"Raman scattering of 5145\AA argon laser radiation by two magnons in the perovskite antiferromagnet KNiF_3 has been observed. At low temperature, the spectrum of the scattered light is in excellent agreement with a Green's function theory for a perovskite with $S = 1$, and nearest-neighbor exchange constant $J = 71.0 \pm .8 \text{ cm}^{-1}$. If the effects of anisotropy, obtained from far-infrared AFMR measurements, are included, the value of J is changed only slightly, decreasing $\sim .5 \text{ cm}^{-1}$. The line shape and position were also observed as a function of temperature. A comparison is made with similar scattering observed in RbMnF_3 ($S = 5/2$) and in related magnetic Ni^{2+} fluorides."

S. R. Chinn
H. J. Zeiger
J. R. O'Connor

2. Linear Wavevector Dispersion in the Shear-Wave Phase Velocity in α -Quartz

Certain optically active crystals may exhibit linear wavevector dispersion in the transverse acoustic branches. Along the c-axis in α -quartz, the two linearly polarized shear waves have equal velocities in the limit $q_z \rightarrow 0$. This degeneracy is lifted proportional to wavevector at finite frequencies, and the normal modes are circularly polarized. The phase velocity difference leads to the phenomenon of acoustical activity⁴⁰ in which the displacement vector of a linearly polarized shear wave rotates around the propagation direction. We have observed an ~ 1 -percent velocity difference of two ~ 30 -GHz shear waves along the c-axis in α -quartz by high-resolution backward Brillouin scattering. The upper trace of Fig. III-10 shows the resulting Brillouin doublet; the lower traces demonstrate the selection rules for scattering from the circularly polarized modes. To obtain the maximum wavevector transfer together with adequate spectral and angular resolution, 180° scattering is employed. Backscattering from shear waves is observable in α -quartz (but not in higher symmetry crystals) because of an allowed Pockel's tensor component p_{14} . The magnitude of the velocity splitting may be extrapolated from recent neutron scattering data.

A. S. Pine

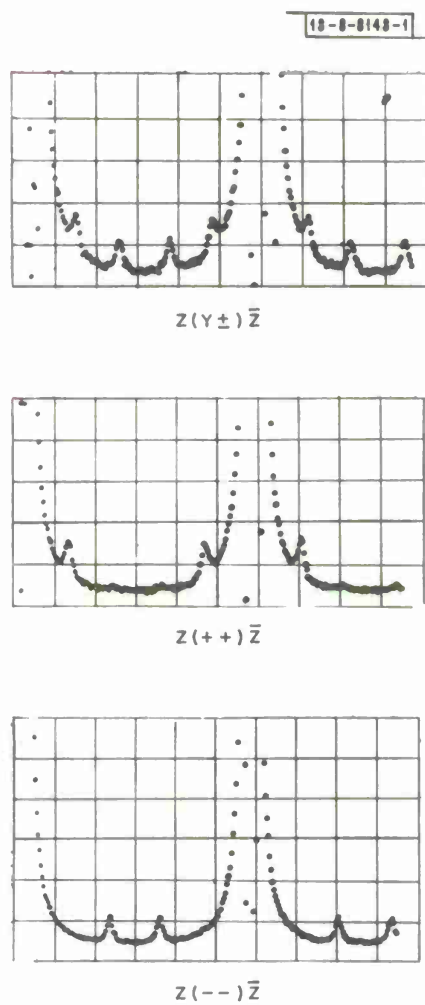


Fig. III-10. Brillouin scattering from shear-wave doublet in α -quartz.
 $\lambda_0 = 5017 \text{ \AA}$, $\theta = 180^\circ$, FSR = 1500 MHz, and $\nu_T = 28.9 \text{ GHz}$.

REFERENCES

1. Solid State Research Report, Lincoln Laboratory, M.I.T. (1968:2), p. 37, DDC AD-672961, H-888.
2. J.P. Van Dyke and F. Herman, Bull. Am. Phys. Soc. 13, 413 (1968); F. Herman, private communication.
3. B. L. Booth and A. W. Ewald, Phys. Rev. 168, 796 (1968).
4. E. O. Kane, The $\vec{k} \cdot \vec{p}$ Method, Physics of III-V Compounds, Vol. 1, edited by R. K. Willardson and A. C. Beer (Academic Press, New York, 1966),
5. B. L. Booth and A. W. Ewald, Phys. Rev. 168, 805 (1968).
6. Solid State Research Report, Lincoln Laboratory, M.I.T. (1967:4), p. 31, DDC AD-665465, H-873.
7. D. K. Wilson and G. Feher, Phys. Rev. 124, 1068 (1961).
8. H. Brooks, Advances in Electronics and Electron Physics, Vol. 7, edited by L. Marton (Academic Press, New York, 1955), p. 85.
9. C. Herring, Bell System Tech. J. 34, 237 (1955), Eq. (C6).
10. D_s is called E_2 by Brooks (in Ref. 8) and Ξ_u by Herring (in Ref. 9).
11. W. E. Krag, W. H. Kleiner, H. J. Zeiger and S. Fischler, Bull. Am. Phys. Soc. 9, 705 (1964).
12. W. E. Krag, W. H. Kleiner, H. J. Zeiger and S. Fischler, J. Phys. Soc. Japan 21S, 230 (1966), DDC AD-646490.
13. Solid State Research Report, Lincoln Laboratory, M.I.T. (1967:4), p. 31, DDC AD-665465, H-873.
14. D. K. Wilson and G. Feher, Phys. Rev. 124, 1068 (1961).
15. W. Kohn and J. M. Luttinger, Phys. Rev. 98, 915 (1955).
16. R. L. Aggarwal, Solid State Commun. 2, 163 (1964).
17. R. L. Aggarwal and A. K. Ramdas, Phys. Rev. 140, A1246 (1965).
18. G. B. Wright and A. Mooradian, Phys. Rev. Letters 18, 608 (1967), DDC AD-653363.
19. J. O. Dimmock and G. B. Wright, Phys. Rev. 135, A821 (1964).
20. K. F. Cuff, et al., Proceedings of the 7th International Conference on the Physics of Semiconductors, Paris, 1964 (Dunod, Paris, and Academic Press, New York, 1965), p. 677.
21. J. O. Dimmock, I. Melngailis and A. J. Strauss, Phys. Rev. Letters 16, 1193 (1966), DDC AD-642225.
22. J. Feinleib, W. J. Scouler, J. O. Dimmock, J. Hanus, T. B. Reed and C. R. Pidgeon, Phys. Rev. Letters 22, 1385 (1969); C. R. Pidgeon, J. Feinleib, W. J. Scouler, J. Hanus, J. O. Dimmock and T. B. Reed, Solid State Commun. 7, No. 18, 1323. (September 1969).
23. V. L. Moruzzi and D. T. Teany, Solid State Commun. 1, 127 (1963); G. Busch, P. Junod, R. G. Morris and J. Muheim, Helv. Phys. Acta 37, 637 (1964).
24. G. Busch, J. Appl. Phys. 38, 1386 (1967).
25. W. J. Scouler, J. Feinleib, J. O. Dimmock and C. R. Pidgeon, Solid State Commun. (in press).
26. J. Hanus, J. O. Dimmock and J. Feinleib, Fifteenth Annual Conference on Magnetism and Magnetic Materials (to be published in J. Appl. Phys., March 1970).
27. G. Busch, P. Junod, R. G. Morris and J. Muheim, Helv. Phys. Acta 37, 637 (1964).

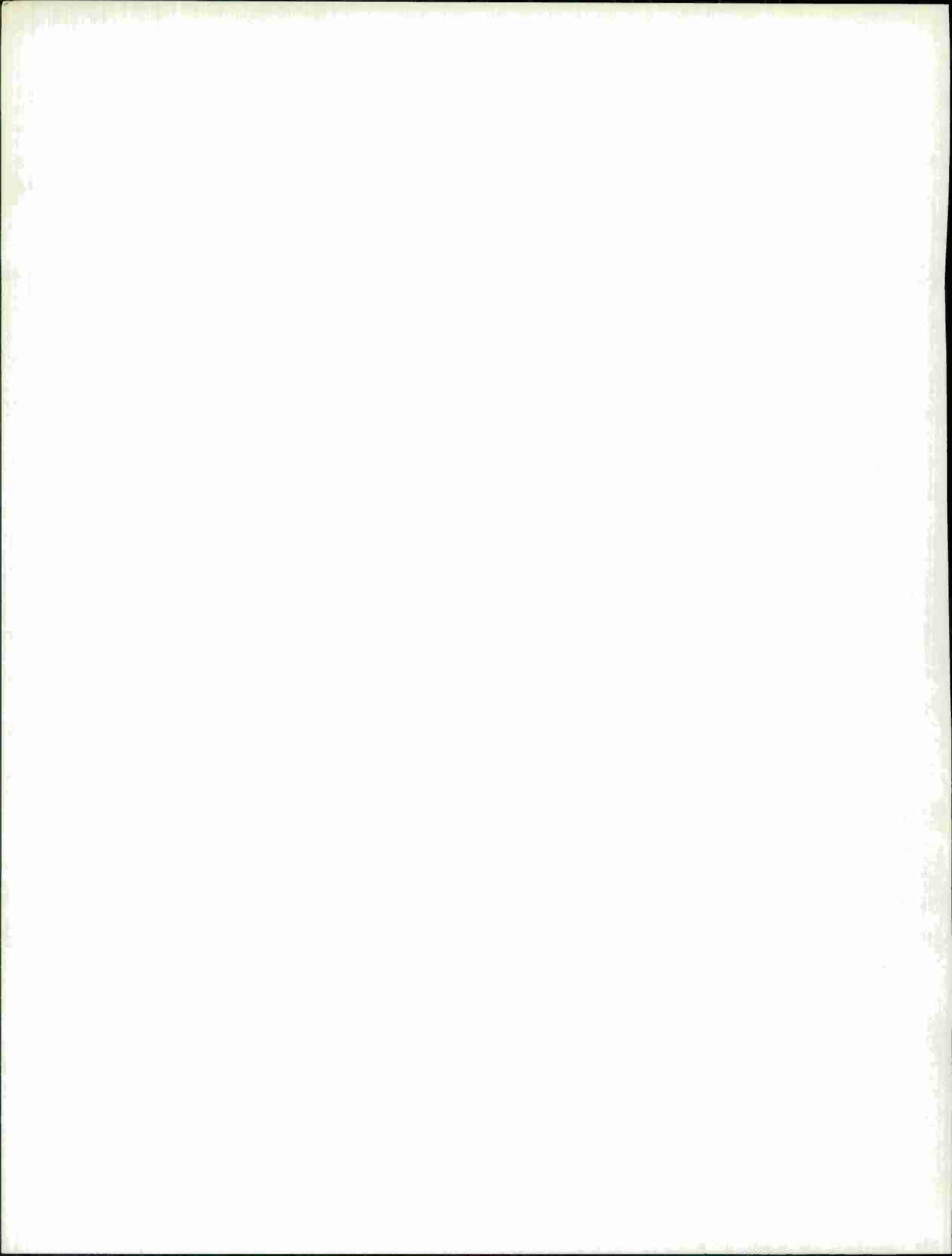
Section III

28. T.R. McGuire and M.W. Shafer, J. Appl. Phys. 35, 984 (1964).
29. J. Feinleib and C.R. Pidgeon (to be published).
30. F. Jellinek, Acta Cryst. 10, 620 (1957).
31. B. van Laar, Phys. Rev. 156, 654 (1967).
32. H. Haraldsen and A. Neuber, Z. anorg. u. allgem. Chem. 234, 337 and 372 (1937).
33. K. Dwight, R.W. Germann, N. Menyuk and A. Wold, J. Appl. Phys. 33, 1341 (1962).
34. D.H. Lyons and T.A. Kaplan, Phys. Rev. 120, 1580 (1960).
35. R.B. Flippen and F.J. Darnell, J. Appl. Phys. 34, 1094 (1963).
36. T. Kamigaichi, T. Okamoto, N. Iwata and E. Tatsumoto, J. Phys. Soc. Japan 21, 2730 (1966).
37. M. Yuzuri, T. Hirone, H. Watanabe, S. Nagasaki and S. Maeda, J. Phys. Soc. Japan 12, 385 (1957).
38. C.F. van Bruggen and F. Jellinek, Colloq. Int. Centre Mat. Rech. Sci. No. 157, 32 (1967).
39. M. Sparks, Phys. Rev. Letters 22, 1111 (1969).
40. D.L. Portigal and E. Burstein, Phys. Rev. 170, 673 (1968).

DOCUMENT CONTROL DATA - R&D

(Security classification of title, body of abstract and indexing annotation must be entered when the overall report is classified)

1. ORIGINATING ACTIVITY (Corporate author)		2a. REPORT SECURITY CLASSIFICATION	
Lincoln Laboratory, M. I. T.		Unclassified	
		2b. GROUP	
		None	
3. REPORT TITLE			
Solid State Research			
4. DESCRIPTIVE NOTES (Type of report and inclusive dates)			
Quarterly Technical Summary - 1 August through 31 October 1969			
5. AUTHOR(S) (Last name, first name, initial)			
Tannenwald, Peter E.			
6. REPORT DATE		7a. TOTAL NO. OF PAGES	7b. NO. OF REFS
15 November 1969		64	82
8a. CONTRACT OR GRANT NO.		9a. ORIGINATOR'S REPORT NUMBER(S)	
AF 19 (628)-5167		Solid State Research (1969:4)	
b. PROJECT NO.		9b. OTHER REPORT NO(S) (Any other numbers that may be assigned this report)	
649L		ESD-TR-69-336	
c.			
d.			
10. AVAILABILITY/LIMITATION NOTICES			
This document has been approved for public release and sale; its distribution is unlimited.			
11. SUPPLEMENTARY NOTES		12. SPONSORING MILITARY ACTIVITY	
None		Air Force Systems Command, USAF	
13. ABSTRACT			
This report covers in detail the solid state research work at Lincoln Laboratory for the period 1 August through 31 October 1969. The topics covered are Solid State Device Research, Materials Research, and Physics of Solids.			
14. KEY WORDS			
solid state devices materials research magnetism Raman scattering		infrared crystal growth x-ray scattering laser scattering	
		electronic band structure magneto-optical research Brillouin scattering magnetic semiconductors	



Printed by
United States Air Force
L. G. Hanscom Field
Bedford, Massachusetts

